HORIZON 2020

HORIZON 2020 RESEARCH AND INNOVATION FRAMEWORK PROGRAMME OF THE EUROPEAN ATOMIC ENERGY COMMUNITY

Nuclear Fission and Radiation Protection 2018 (NFRP-2018-4)

Project acronym: **SANDA**

Project full title: **Solving Challenges in Nuclear Data for the Safety of European Nuclear facilities**

Grant Agreement no.: **H2020 Grant Agreement number: 847552**

Work package N°: **WP5**

Identification N°: **D 5.12**

Type of document: **Deliverable**

Title: **Report on the integral experiment at TAPIRO**

Dissemination Level: **PU**

Reference:

Status: ***VERSION 1***

Comments:

	Name	Partners	Date	Signature
Prepared by:	V. Fabrizio L. Falconi	ENEA, CEA	10-06-2024	
WP leader:	R. Jacqmin	CEA	10-06-2024	JACQMIN Robert 116318 Signature numérique de JACQMIN Robert 116318 Date : 2024.08.30 15:53:39 +02'00'
IP Co-ordinator:	E. González	CIEMAT	14-08-2024	Signed by GONZALEZ ROMERO ENRIQUE MIGUEL - DNI ***3708** at 30/08/2024 with a certificate isued by AC Sector Público

Executive summary

The main issue of the R&D on nuclear waste management is the radiotoxicity reduction of the nuclear spent fuel, which is mainly due to some elements, i.e. plutonium and other Minor Actinides (MAs) as neptunium, americium and curium. By fissioning these elements in appropriate nuclear reactors they can be eliminated. A deeper knowledge in the nuclear data of these MAs is of primary importance in order to deal with their transmutation.

Focusing on this goal, the AOSTA (Activation of OSMOSE Sample in TAPIRO) campaign, under the aegis of the NEA Expert Group on Integral Experiments for Minor Actinide Management, is oriented to analyze the feasibility of a MAs irradiation campaign in the TAPIRO Italian fast source research reactor. A fraction of these activities are performed in the framework of WP5 of the EURATOM project SANDA for the validation of Nuclear Data with integral experiments. In particular this report describes the activities for calibration and test of the TAPIRO reactor for its use to perform integral experiments that can validate nuclear data.

The feasibility studies, carried out by calculations modeling the irradiation, in different TAPIRO irradiation channels, of some samples, supplied by CEA and coming from the French experimental campaign OSMOSE and AMSTRAGRAM, containing different type and content of MAs, are shown in this report.

Another open issue is the need to figure out how the response of the MAs reaction rates, essentially capture, is linked to the TAPIRO copper reflector nuclear data. In this work the sensitivity coefficients of some MAs capture rates to Cu cross section variations have been preliminarily estimated by means of both Generalized Perturbation Theory (GPT) and direct approach by deterministic calculations.

Then the Phase 1 of the experimental campaign carried out in October 2021 by CEA and May-June 2022 by ENEA staff is presented and discussed.

Summary

Report on integral experiments at TAPIRO

V. Fabrizio[a], L. Falconi[a], L. Lepore[a], A. Santagata[a], P. Console Camprini [a], R. Combe-Colas[b],

[a]*ENEA, Agenzia per le Nuove Tecnologie, l'Energia e lo Sviluppo Economico Sostenibile, C.R: Casaccia, Italy.*
[b]*CEA, Cadarache, Saint-Paul-lez- Durance, France*

(*) corresponding author: valentina.fabrizio@enea.it

1. Introduction

The TAPIRO fast neutron source reactor at the ENEA Casaccia centre, near Rome, represents a suitable facility for measuring minor actinide spectrum-averaged cross sections. Valuable new validation data have been planned to be provided within the framework of the SANDA project. The subsequent use of this experimental information for nuclear data validation will provide some indication of the remaining gaps to improve evaluated files and meet target performance. Recommendations can be made as to the best course of action to bridge this gap, knowing that there is only a very small number of zero-power experimental reactors still in operation worldwide.

In the frame of the NEA Expert Group on Integral Experiments for Minor Actinide Management [1], a joint collaboration between ENEA (Italian National Agency for New Technologies, Energy and Sustainable Economic Development) and CEA (French Alternative Energies and Atomic Energy Commission) was established with the aim to study the feasibility of a minor actinides (MAs) irradiation campaign in the TAPIRO fast neutron source research reactor located at the ENEA Casaccia center [2]. A fraction of this research has been performed and partially financed in the framework of the SANDA Euratom project. On the basis of neutron transport calculation results, obtained by both deterministic and Monte Carlo methods, an estimate of the irradiated samples counting levels from the AOSTA (Activation of Osmose Samples in TApiro) experimental campaign has been evaluated in previous works [3].
The aim of these calculations is to evaluate the possibility to fulfill activation measurements in TAPIRO, in order to access capture cross sections of MAs, analyzing the (n,γ) activation chains. The feasibility of this experiment depends on various factors such as the activity level of the samples after irradiation (that influence the cooling time after which it would be possible to extract the samples from the system without radiological risks for the operators) and the energy of the γ-rays emitted. This last information is fundamental for the counting rate estimation, and it influences the necessary detector type.
In this document are shown the preliminary results obtained by deterministic and probabilistic calculations modeling the irradiation. The deterministic TAPIRO model take into account 4 different TAPIRO irradiation channels (core centre, equivalent to tangential channel, centre reflector and centre shield), to compare with the probabilistic model in which all the irradiation channels have been modeled. For this preliminary analysis six OSMOSE (Oscillation in MINERVE of isotope in 'Eupraxic' Spectra)[1] samples, loaded with different contents of MAs, have been chosen, according to the CEA.
Due to a possible contamination of the expected gamma spectra by the UO_2 matrix (OSMOSE samples), additional AmO_2 samples from IRMM, used in the AMSTRAMGRAM program in MINERVE [3], will also be analyzed for the irradiation in TAPIRO and their results are also shown.
On the basis of neutron transport calculational results, obtained by deterministic ERANOS [4] code, an estimate of the irradiated samples counting levels from the AOSTA [5] experimental campaign, taking into account both geometry and efficiency of the counting system, is provided using the FISPACT 2007 inventory code [6]. The average microscopic capture cross sections obtained by the Monte Carlo codes Serpent [7] and MCNP [8, 9] (the latter with its in-house variance reduction algorithm [10, 11]), are compared with the ERANOS results. Whereas the

[1] This program was finalized to measure the integral absorption rates of minor actinides using the oscillation technique in MINERVE, a CEA research reactor located in Cadarache. The program was a DOE-CEA collaboration.

preliminary reactivity associated with the insertion of some OSMOSE and IRMM samples into the TAPIRO reactor is evaluated by MCNP 6.1 [10].
Another open issue to carry out the experimental campaign is the need to figure out how the response of the MAs reaction rates, essentially capture, is linked to copper reflector nuclear data uncertainties. To preliminary address this issue, in this work an analysis of some MAs capture reaction rates sensitivity due to a 2% copper density reduction in the whole TAPIRO reflector is carried out. The 2% variation is chosen to be representative of an uncertainty on the nuclear data for copper. Calculations are performed by means of GPT (Generalized Perturbation Theory) [7], implemented in the deterministic code ERANOS. The study has involved two different MAs isotopes: Am^{241} and Np^{237}. GPT results have been compared with those coming from a direct approach.
Preliminary characterization of the TAPIRO neutron field carried out in 2021-2022 experimental campaigns, by means of fission chambers measurements (CEA staff) and activation foils for characterization of the tangential channel (ENEA staff) are also presented.

2. The TAPIRO fast neutron source research reactor

TAPIRO (**TA**ratura **Pi**la **R**apida a potenza zer**O** - Fast Pile Calibration at 0 Power) is a fast neutrons source research reactor located at C.R ENEA-CASACCIA (Italy). The project, entirely developed by ENEA staff, is based on the general concept of AFSR (Argonne Fast Source Reactor - Idaho Falls). It was built to support an experimental program on fast reactors and it is in operation since 1971.TAPIRO is currently used, in addition to education and training, for experimental programs in support of different research fields like nuclear data, nuclear fusion, aerospace industry.

The reactor has a maximum power of 5 kW with a neutron flux around $4 \cdot 10^{12}$ n/(cm^2·s) in the center of the core. The core is cylindrical with a diameter of about 12 cm and a similar height. It is made of metallic uranium (98.5 % uranium and 1.5 % molybdenum) with an enrichment of 93.5 % in U^{235}. It consists of 2 parts: the upper part is fixed while the lower one is movable. The core is surrounded by a double layer of a copper reflector and by an external borate concrete biological shield. The core is cooled by helium. The reactor is equipped with 2 shim rods, 2 safety rods and a regulating rod. These rods are made of the same material as the reflector, i.e. copper, and the reactor is controlled by increasing or decreasing the neutron leakage. The system has different experimental channels with various diameters. A horizontal section of the reactor is shown in Figure 1.

Figure 1. TAPIRO horizontal section.

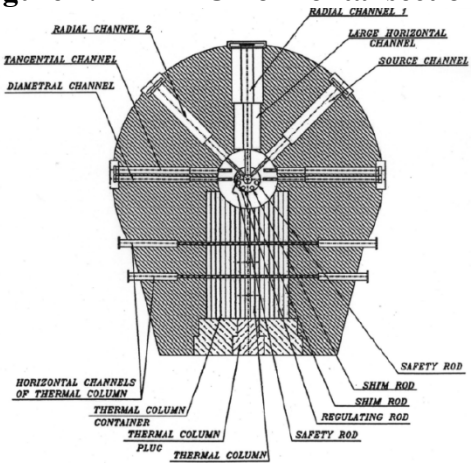

3. Energy averaged capture cross sections evaluation.

Neutron transport calculations have been performed by two different methodologies, deterministic by the ERANOS code, and stochastic by both the Monte Carlo codes SERPENT

[8] and MCNP [9, 10]. Figure 2 details a view of the TAPIRO geometry implemented for the calculations with the two methodologies.

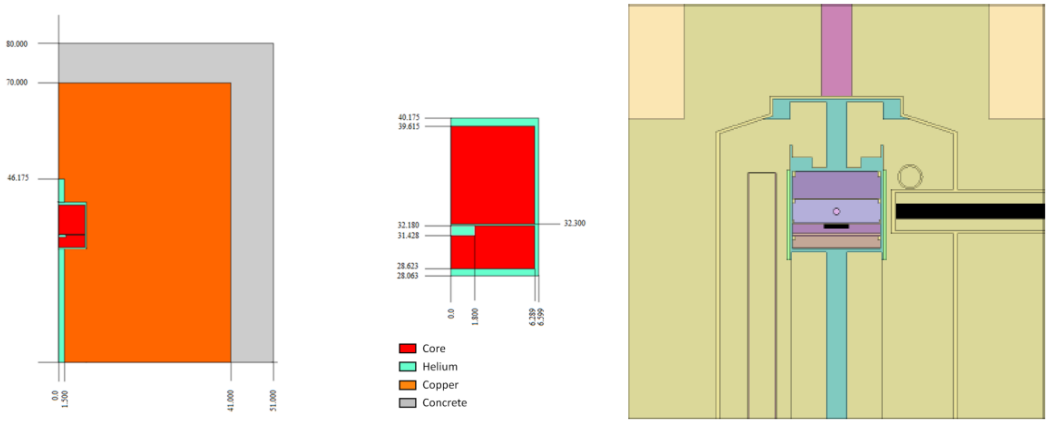

(a) - RZ ERANOS model (b) - Serpent model

Figure 2. ERANOS and Serpent-MCNP TAPIRO calculation models

Neutron fluxes, energy spectra and reaction rates have been evaluated for several minor actinides in correspondence between different radial positions in the experimental channels considered for this experiment: diametral channel, tangential channel, radial-1 channel. Subsequently position-dependent average microscopic capture cross sections have been calculated to predict the impact on their values of the spectral variations across the system. Average capture microscopic cross sections $\bar{\sigma}_c(\mathbf{r})$ are defined as:

$$\bar{\sigma}_c(\mathbf{r}) = \frac{\int \sigma_c(\mathbf{r},E)\varphi(\mathbf{r},E)dE}{\int \varphi(\mathbf{r},E)dE} \tag{1}$$

with φ the neutron flux. Figure 3 shows the neutron spectra, while Figure 4 and Figure 5 reproduce the fission and capture cross section of the main Minor Actinides respectively. As it can be seen, the 3 spectra exhibit different behaviors: the central and reflector spectra are almost the same (with a higher epithermal part) while the shield position presents a thermal contribution around 20% of the total flux. Figure 3 indicates that an optimized use of the 3 irradiation positions would enable to properly cover the whole range of interest. This will be confirmed by a complementary reaction rates sensitivity analysis.

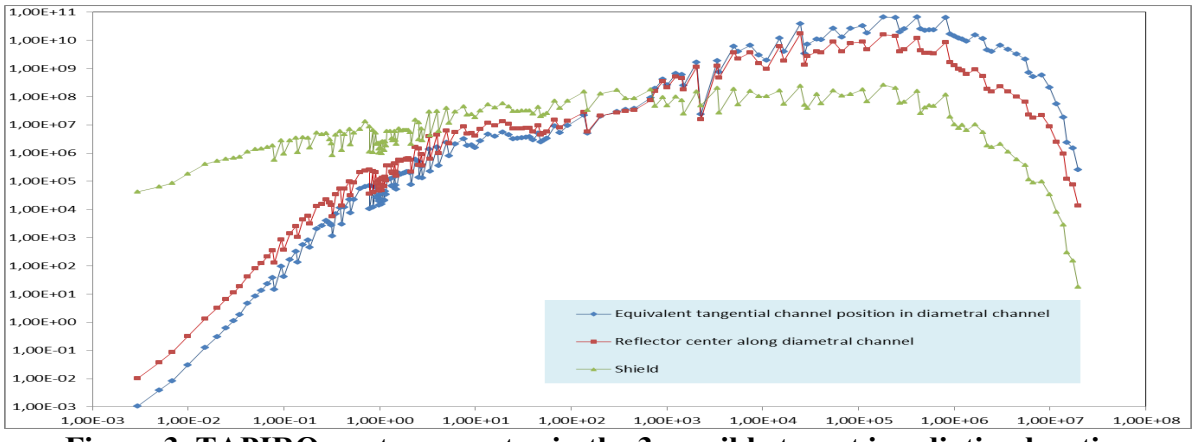

Figure 3. TAPIRO neutron spectra in the 3 possible target irradiation location

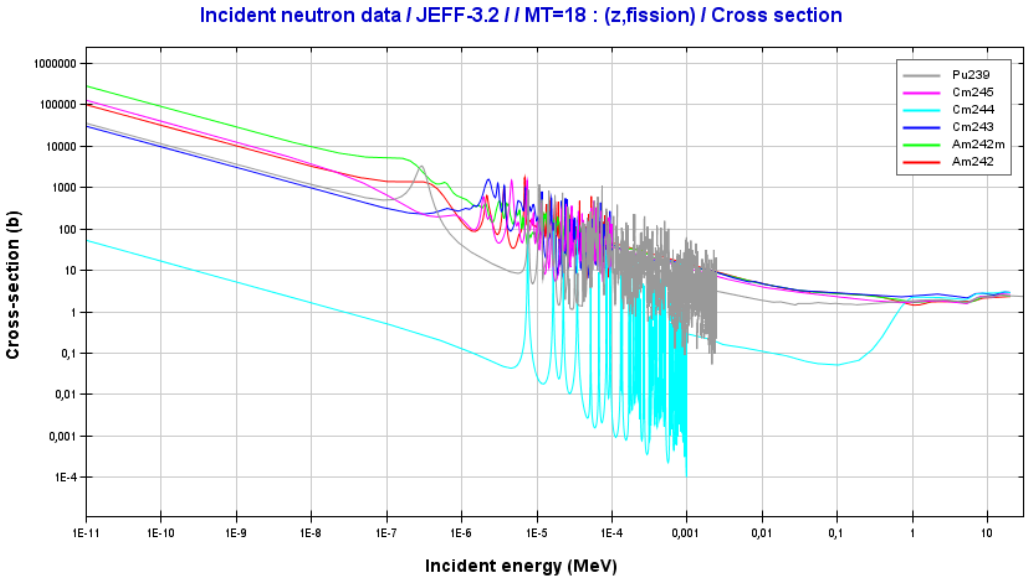

Figure 4. Fission cross sections of the main Minor Actinides

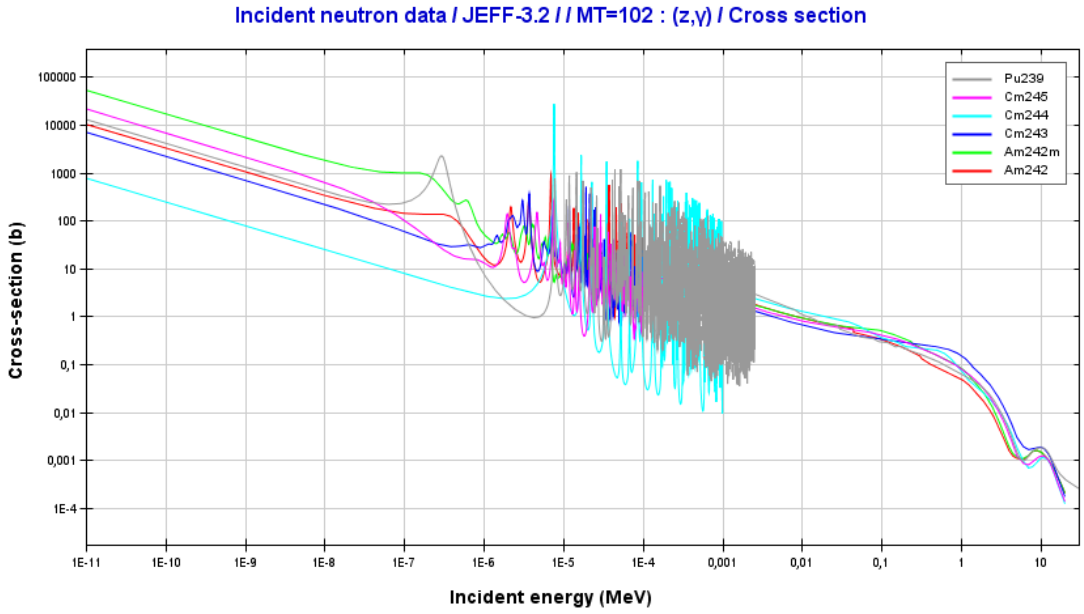

Figure 5. Capture cross sections of the main Minor Actinides

As an example, the behavior across the system of the average capture microscopic cross sections ($<\sigma_c(\varphi)>/<\varphi>$) for the minor actinide ^{241}Am, calculated with both ERANOS, SERPENT and MCNP, employing the Jeff – 3.1 data library, is shown in Figure 6.

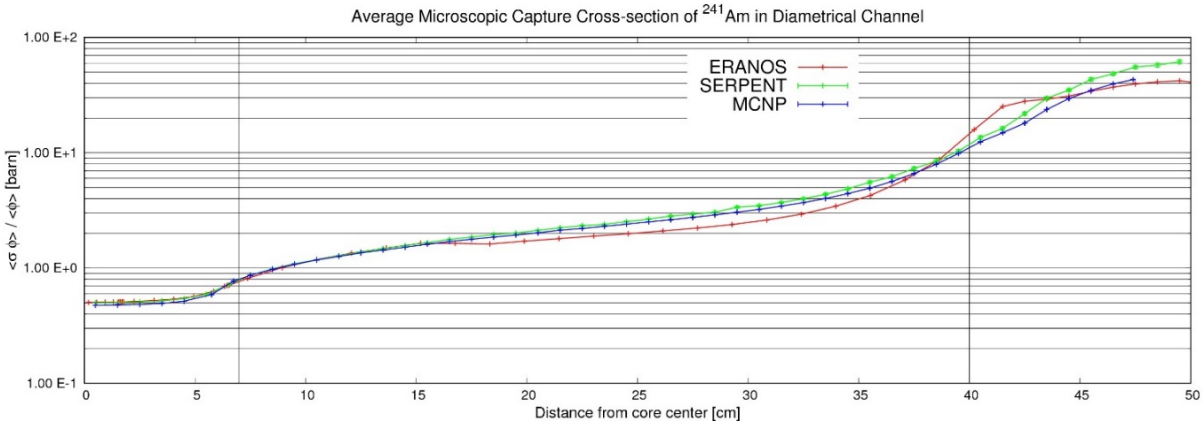

Figure 6. ^{241}Am average microscopic capture cross section in the diametral channel.

A satisfactory agreement can be observed, also for the other samples, between ERANOS, Serpent and MCNP**.**

4. Evaluation of the counting rates after irradiation of the OSMOSE samples

The selected OSMOSE samples contain ^{237}Np, ^{242}Pu, ^{241}Am, ^{243}Am in a double Zircaloy sheath (Figure 7). The matrix for all the samples is composed of natural uranium.

Figure 7. OSMOSE samples.

In agreement with the ordinary daily working hours of TAPIRO staff, it was assumed to irradiate these samples following a weekly scheme characterized by 5 hours of irradiation and 19 hours of cooling repeated for 4 times and then 5 hours of irradiation and 2 hours of cooling. Activity values have been evaluated after these last 2 hours of cooling (Figure 8).

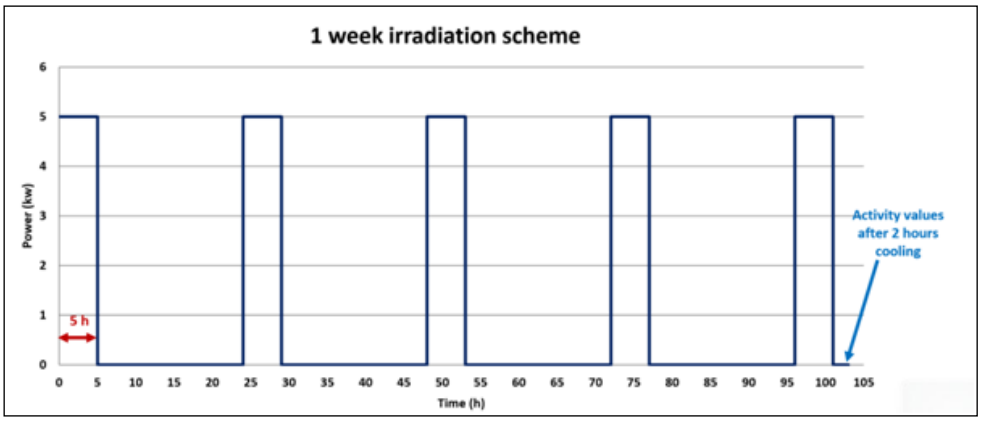

Figure 8. Irradiation scheme

Three sample positions have been considered along the diametral channel: r = 12.07 cm (near the core), 24.58 cm (about reflector center) and 45.4 cm (entrance of the thermal column), see Figure 2(a). In correspondence between such positions the activity values have been calculated by the FISPACT code [7], for each OSMOSE sample, associated to the irradiation scheme shown in Figure 8. The obtained results, by using the ERANOS neutron flux results for this preliminary analysis, are shown in Table 1.

	Position	r = 12.07 cm	r = 24 .58 cm	r = 45.5 cm
OSMOSE Samples	ϕ (n·cm^{-2}·s^{-1})	6.94E+11	1.74E+11	8.79E+09
Np237	$\sigma_{c,Np237}$ (barn)	1.04	1.73	19.57
	A (Bq)	2.04E+08	8.49E+07	4.85E+07
Pu242	$\sigma_{c,Pu242}$ (barn)	0.34	0.62	22.48
	A (Bq)	1.15E+08	5.30E+07	9.68E+07
Am241	$\sigma_{c,Am241}$ (barn)	1.32	2.06	32.61
	A (Bq)	1.15E+08	4.50E+07	3.61E+07
Am243	$\sigma_{c,Am243}$ (barn)	1.13	1.83	33.40
	A (Bq)	2.10E+07	8.10E+06	7.14E+06

Table 1. Energy average cross sections and activity levels for samples at different position in TAPIRO.

The estimation of the counting rate [counts/s] for each sample and position was evaluated by the relationship:

$$C = A \cdot I_\gamma \cdot \varepsilon \tag{2}$$

with A the activity level in Bq computed by FISPACT, I_γ the intensity of the γ or X emission [%], and ε the geometric efficiency of the sample-HPGe detector geometry [%].
The geometric efficiency ε depends on the semiconductor type used for detection and on the overall experimental geometrical arrangement. In our case, was considered a n-type coaxial HPGe detector made of high purity germanium, showing high precision and efficiency for both γ and X rays in the energy range 3 keV÷10 MeV. The geometric efficiency has been evaluated by Monte Carlo MCNP code modeling the arrangement of the counting system (Figure 9).

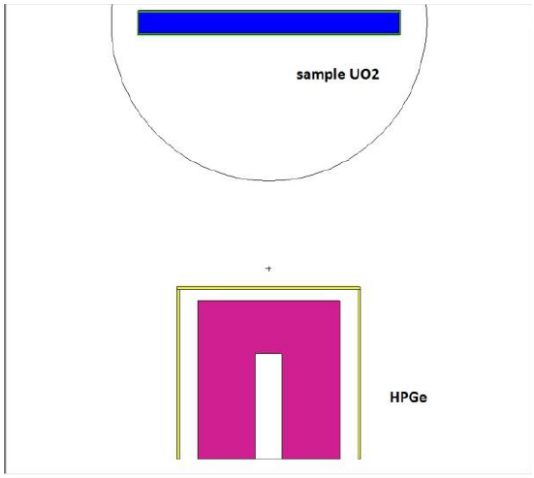

Figure 9. MCNP modeling of the counting system.

Table 2 summarizes the results obtained. One details, for each sample and position, the γ or X rays characteristics (energy and intensity), the geometric efficiency and the counting level obtained by relationship (2).

	Position	r = 12.07 cm	r = 24 .58 cm	r = 45.5 cm
OSMOSE Samples	ϕ (n·cm^{-2}·s^{-1})	6.94E+11	1.74E+11	8.79E+09
Np237	Np238 E γ (keV)	984.45	984.45	984.45
	γ Intensity (%)	25.19	25.19	25.19
	ε Detection (%)	0.186	0.186	0.186
	C (cps)	95487	39779	22738
Pu242	Pu243 E γ (keV)	84	84	84
	γ Intensity (%)	23.10	23.10	23.10
	ε Detection (%)	0.021	0.021	0.021
	C (cps)	5559	2572	4698
Am241	Am 242 E $X_{K\alpha1}$ (keV)	103.374	103.374	103.374
	$X_{K\alpha1}$ Intensity (%)	5.70	5.70	5.70
	ε Detection (%)	0.107	0.107	0.107
	C (cps)	7014	2745	2204
Am243	Am244 E γ (keV)	743.971	743.971	743.971
	γ Intensity (%)	66.00	66.00	66.00
	ε Detection (%)	0.213	0.213	0.213
	C (cps)	29466	11391	10032

Table 2. Counting rates for the selected OSMOSE samples in TAPIRO.

The counting rate levels shown in Table 3 seem to predict the feasibility of the AOSTA experimental campaign although, as evident, a more detailed analysis is needed in the next future to confirm these promising preliminary results.

5. Evaluation of the counting rates after irradiation of the IRMM samples

The IRMM samples, Figure 10, contain ^{241}Am (chemical form Am_2O_3) in a single aluminum sheath (Table 3). The matrix for all the samples is composed of Al_2O_3. The material balance of those samples is given in Table 3. The activity of one sample is about 5 GBq.

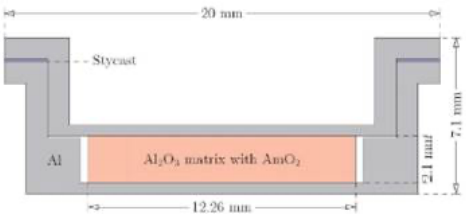

Figure 10. IRMM AmO_2 samples for the AMSTRAMGRAM program.

Series	Ref.	Dopant	Mass pellet (g)	^{241}Am Mass (mg)	Al_2O_3 Mass (g)
Americium	IRMM-1	$^{241}AmO_2$	0.342	32.23 ± 0.19	0.305
	IRMM-2	$^{241}AmO_2$	0.442	42.15 ± 0.25	0.394
	IRMM-3	$^{241}AmO_2$	0.428	40.32 ± 0.25	0.382
	IRMM-4	$^{241}AmO_2$	0.435	40.98 ± 0.25	0.388
	IRMM-5	$^{241}AmO_2$	0.448	41.21 ± 0.25	0.401
	IRMM-6	$^{241}AmO_2$	0.447	42.10 ± 0.25	0.399
	IRMM-7	$^{241}AmO_2$	0.444	41.84 ± 0.25	0.396
	IRMM-8	$^{241}AmO_2$	0.441	41.46 ± 0.25	0.394
	IRMM-9	$^{241}AmO_2$	0.447	42.09 ± 0.25	0.399
	IRMM-11	$^{241}AmO_2$	0.451	42.38 ± 0.25	0.408
	IRMM-13	-	0.395		0.395
	IRMM-14	-	0.407		0.407
	IRMM-15	-	0.385		0.385

Table 3. Material balance of the AMSTRAMGRAM candidate samples to be activated in TAPIRO (The activation evaluations have been performed for all IRMM samples although only some of them will be actually available for the program.)

Contrary to the OSMOSE samples, the amount of Am in each sample is high enough to consider only a daily irradiation characterized by 5 hours of irradiation and 2 hours of cooling. Activity values have been evaluated after these last 2 hours of cooling (Figure 8).
Due to their diameter, their irradiation can only be foreseen in the tangential channel. The counting rates on ^{242}Am are given in Table 4.
Because of the very strong activity of ^{241}Am (~3.6 10^9 Bq for sample IRMM-1), the competition between ^{242}Am $X_{k\alpha 1}$ ray at 103.37 keV and ^{241}Am gamma ray at 102.98 keV has to be taken into account. Analogous calculations as above give a counting rate of 2288 c/s for this particular gamma ray. The measurement process will be adapted in order to precisely unfold the two peaks, and also take care of the overall background:

- The strong ^{241}Am activity should be screened in order to limit the detection dead time to a few per cents, for instance by using a very narrow collimator.
- The background activity should be carefully subtracted from the spectra, for instance by following the ^{242}Am decay over several days and then analyzing differences between two consecutive spectra.

AMSTRAMGRAM Samples	Position	r = 12.07 cm
	($n \cdot cm^{-2} \cdot s^{-1}$)	7.44E+11
	Am 242 E $X_{K\alpha 1}$ (keV)	103.374
	$X_{K\alpha 1}$ Intensity (%)	5.70
	ε Detection (%)	0.287
IRMM_1	C (cps)	1793
IRMM_2	C (cps)	2344
IRMM_3	C (cps)	2341
IRMM_4	C (cps)	2279
IRMM_5	C (cps)	2292
IRMM_6	C (cps)	2341
IRMM_7	C (cps)	2326
IRMM_8	C (cps)	2305
IRMM_9	C (cps)	2341
IRMM_11	C (cps)	2357

Table 4. Counting rates for the selected AMSTRAMGRAM samples in TAPIRO (ERANOS neutron fluxes).

6. Evaluation concerning the reactivity associated with the samples.

An evaluation concerning the reactivity associated with the insertion of some OSMOSE and IRMM samples in the TAPIRO channels has been performed.
The considered positions in the standard TAPIRO core configuration (see Fig. 11) are the following (see Fig. 12), all the positions being at locations as close as possible to the core center:

1. OSMOSE samples in Tangential and Radial-1 channels (see Fig. 12) (red circles in Fig. 12);
2. IRMM samples in Diametral, Tangential and Radial-1 channels (see Fig. 14) (blue circles in Fig.12).

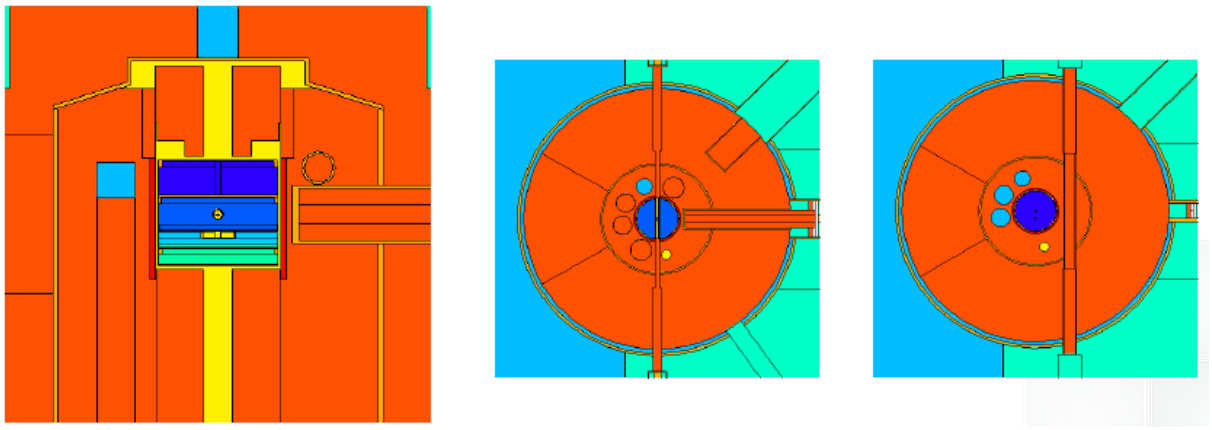

Figure 11. TAPIRO standard configuration

Name	Position	Penetration	Useful diameter
Diametral channel (D.C.)	Piercing. Horizontal. Diametral in the core.	Inner and outer fixed reflector. Core.	10 mm in core
Tangential channel	Piercing. Horizontal. 50 mm above core mid-plane. Parallel to D.C. 106 mm from core axis.	Inner and outer fixed reflector.	30 mm in reflector
Radial channel 1 (R.C.1)	Radial. Horizontal on core mid-plane, at 90° with respect to D.C.	Inner and outer fixed reflector, up to 93 mm from core axis.	56 mm in reflector
Radial channel 2	Radial. Horizontal on core mid-plane, at 50° with respect to R.C.1.	Outer fixed reflector, up to 228 mm from core axis.	80 mm in reflector
Grand Horizontal Channel (G.H.C.)	Radial. Concentric with R.C.1.	Up to reflector outer surface	400 mm near reflector
Grand Vertical Channel (G.V.C.)	Above core, on the same axis.	Outer fixed reflector, up to 100 mm from upper core base.	800÷900 mm in reflector
Thermal column	Horizontal.	Shield, up to outer reflector	110x116x160 cm³
Irradiation cavity	On safety plug upper base.	7.4 mm	33 mm

Figure 12. Irradiation channels for reactivity evaluation.

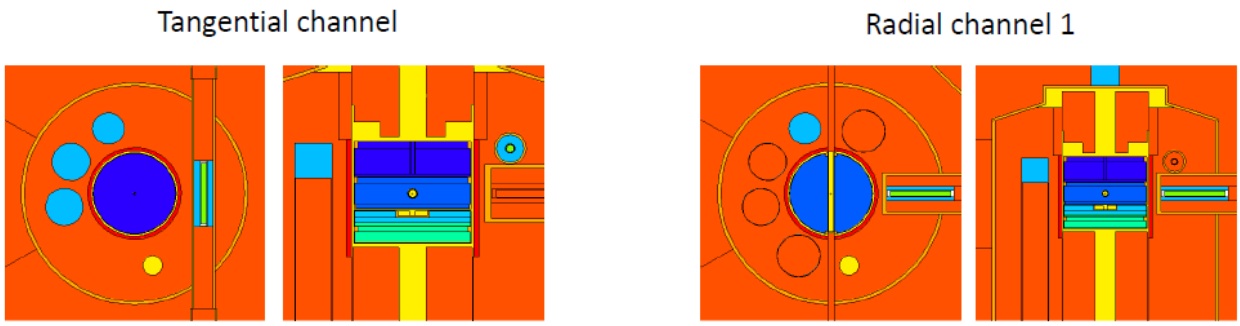

Figure 13. OSMOSE sample modeling in MCNP.

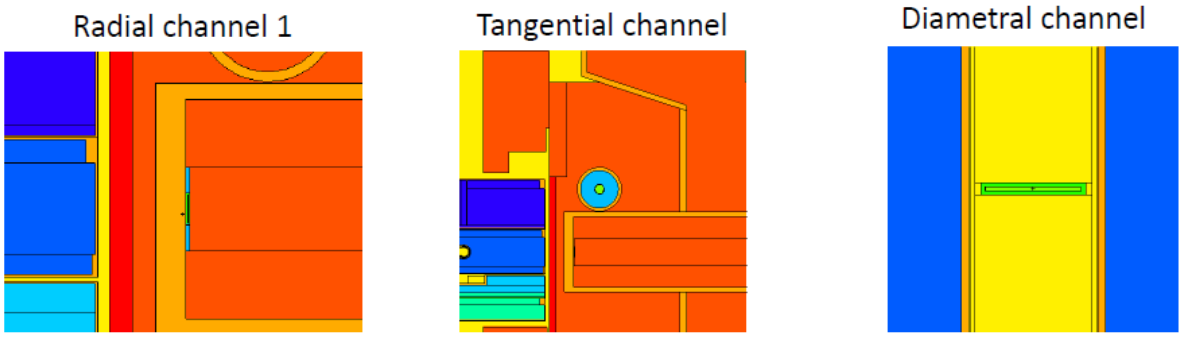

Figure 14. IRMM sample modeling in MCNP.

In particular, the selected samples are the following:

1. for the OSMOSE case the sample Am241 containing 0.2 grams of ^{241}Am
2. for the IRMM case the sample IRMM-1 containing 32.23 mg of ^{241}Am (see Table 3).

Details of the Perturbation Calculations and Results

The Monte Carlo code MCNP6.1 [10] was employed with JEFF 3.1 cross-sections. MCNP6.1 allows three ways of estimating reactivity perturbations:

1) In a direct fashion (i.e. the difference between the responses from two calculations, one with the reference configuration, the other with the perturbed configuration).
2) In a single calculation with the "PERT" card (employs the first and second order differential operator technique) [12].
3) In a single calculation with the "KPERT" card (employs the adjoint flux in a bilinear functional) [13].

Note that in both perturbation approaches, we generated histories in a reference tracking configuration which was halfway (in terms of material atomic densities) between the standard, or reference, TAPIRO configuration (Tangential and Radial-1 channels filled with copper and Diametral channel filled with helium) and OSMOSE or IRMM inserted in one of the channels. Simultaneous perturbations were then made one way to the reference TAPIRO configuration and the other way to TAPIRO with OSMOSE or IRMM.

Each approach embodies some difficulties:

- The direct approach is limited by the size of the perturbation – in the AOSTA context it turns out that the change of reactivity when inserting OSMOSE could be calculated in this way whilst the change of reactivity when inserting IRMM could not.
- The differential operator technique assumes that the fundamental mode is not perturbed. It turns out that this assumption is valid for both OSMOSE and IRMM.
- The bilinear weighting method introduces an approximation in the handling of the scattering, although it seems in this problem not to be an issue. More importantly here, statistics are far worse than with the differential operator technique.

The reference value of k_{eff} for the standard, or reference, TAPIRO configuration was 0.99928 ± 0.00001 (one standard deviation).

OSMOSE

We employed the direct approach for OSMOSE in both the Tangential and Radial-1 channels. In the Tangential channel, we verified the direct results with both the "PERT" and "KPERT" algorithms. The results (in terms of reactivity variation Δρ in pcm with one standard deviation statistical error) are in Table 5:

Case	Tangential channel			Radial-1 channel		
	Track Ref. → TAPIRO	Track Ref. → OSMOSE	**TAPIRO → OSMOSE**	Track Ref. → TAPIRO	Track Ref. → OSMOSE	**TAPIRO → OSMOSE**
Direct			**-68 ± 2**			**-33 ± 1**
PERT	+33 ± 0	-38 ± 0	**-71 ± ~0**			
KPERT	+35.1 ± 1.7	-35.1 ± 1.7	**-70.2 ± ~3.4**			

Table 5. OSMOSE Results for Reactivity Variation Δρ in pcm .
("Track Ref." = reference tracking configuration).

Note that:

- the results validate the three approaches – OSMOSE is small enough not to alter the fundamental mode (result confirmed also by the KPERT results) and the scattering approximation in KPERT seems to have no impact.

- the errors on the total perturbations are not given by the code and are therefore estimates.
- nearly all (PERT: >99%; KPERT: 98%) of the reactivity change, TAPIRO → OSMOSE in the tangential channel, is due to the air around OSMOSE. Changing this copper to air introduces nearly all the negative reactivity.

IRMM

As already mentioned IRMM is too small for the difference between the k_{eff}'s of two calculations not to be swamped by the noise. This holds for both the Tangential, Radial-1 and Diametral channels. Therefore, a perturbation approach is required. Furthermore, it turned out that also the KPERT results were too noisy to give any meaningful value for Δk_{eff}. Thus the only possibility was with the PERT card:

Firstly, the default output with the PERT card, employed above for OSMOSE, listing the value of k_{eff} after applying each perturbation defined in the input, only gives the value of the perturbed k_{eff} to the nearest pcm. This is not fine enough for IRMM. Therefore, as an alternative the fission production rate was tallied with the track length estimator in each of the five fuel zones of the TAPIRO core plus in the single americium oxide zone of IRMM. Then the PERT option allows the *differential* change in the unperturbed tally to be output.

Secondly, although each TAPIRO fuel zone consists of a number of geometric cells, the total was requested over all the cells containing the same material. Thus a total of six results (5 TAPIRO fuel zones + IRMM AmO_2) were output for each of the three cell perturbations of IRMM in the Tangential and Radial-1 channels (Am/Cu, clad/Cu and void/Cu cells) or for each of the two cell perturbations of IRMM in the Diametral channel (Am/He and clad/He cells), for each of the two perturbations: reference tracking configuration → TAPIRO and reference tracking configuration → IRMM. This gives a total of 36 results, each with their correctly estimated error, for IRMM in the Tangential and Radial-1 channels and 24 results, each with their correctly estimated error, for IRMM in the Diametral channel. The results must then be summed for each channel to provide the final perturbation result. The estimated error was not available on these sums.

The small size of IRMM meant that the statistical error remained non-negligible, even after using substantial computer resources (see acknowledgement). Therefore, it was desired to provide a correctly estimated error on all the sums so as to have the final results with their proper error. To this end, MCNP6 was patched in an *ad hoc* fashion. The results (in terms of reactivity variation Δρ in pcm with one fractional standard deviation statistical error) in Table 6 were generated with this patched MCNP 6.1 version.

Case	Tangential channel			Radial-1 channel		
	Track Ref. → TAPIRO	Track Ref. → IRMM	**TAPIRO → IRMM**	Track Ref. → TAPIRO	Track Ref. → IRMM	**TAPIRO → IRMM**
PERT	+0.323 ± 3.3%	-0.341 ± 3.1%	**-0.664 ± 3.1%**	+0.463 ± 2.5%	-0.472 ± 2.5%	**-0.935 ± 2.4%**

Case	Diametral channel		
	Track Ref. → TAPIRO	Track Ref. → IRMM	**TAPIRO → IRMM**
PERT	-0.0398 ± 16.1%	+0.0387 ± 16.5%	**+0.0785 ± 16.2%**

Table 6. IRMM Results for Reactivity Variation Δρ in pcm
("Track Ref." = reference tracking configuration)

Note that:

- we assume that IRMM in the diametral channel, due to its very small size, does not perturb the fundamental mode.
- for the Tangential and Radial-1 channels, >98% and ~95% respectively of the reactivity change is due to the air around IRMM. (Changing this copper to air introduces nearly all the negative reactivity.) Instead in the Diametral channel, this zone remains unperturbed (there is helium in TAPIRO in the Diametral channel at the reactor centre). Instead, the americium oxide of IRMM is responsible for approximately 10 times the reactivity change compared with the cladding (and of course the two perturbations have a different sign).
- the greater reactivity perturbation of IRMM in the Radial-1 channel compared with the Tangential channel, reversing the OSMOSE results, is due to geometrical effects (length of OSMOSE compared to IRMM and geometry of the two channels).

In view of the low reactivity levels obtained in these preliminary evaluations for the IRMM-1 sample, the possibility could be considered to stack several samples together to increase the total Am mass.

7. Sensitivity coefficients for copper density reduction.

The TAPIRO research reactor is well suited for minor actinides studies due to its spectrum variety starting from a hard spectrum in the central core, near to fission one, an intermediate spectrum in the copper reflector up to a moderated spectrum in the biological shielding.
The reliability and significance of the measurements carried out in TAPIRO are also influenced by the presence of a copper reflector, a peculiarity of this reactor leading to the variety of spectral zones discussed above. Therefore, to assess the influence of the uncertainty on the reflector properties on the MA measures, the capture reaction rates sensitivities for two different MAs, Am^{241} and Np^{237}, after a 2% copper density reduction in the whole reflector, have been evaluated. Results for both the MAs are in correspondence between four different positions along one of the TAPIRO experimental channels, the diametral channel (at axial reactor mid-plane).
The four different positions analyzed along the diametral channel are: r=0.5 cm near the core centre (P1), r=12.07 cm near the core boundary (P2), r=24.58 cm at about the reflector center (P3) and r=45.5 cm at the entrance of the thermal column (P4).
The energy integrated capture rates variations (total sensitivity), obtained by means of GPT (Generalized Perturbation Theory) [15] using a 49 energy groups grid for the calculations, for each actinide and position considered, are shown in Table 7.

	Integral capture rates variations			
Position / Isotope	0.5 cm	12.07 cm	24.58 cm	45.5 cm
Am^{241}	-3.24E-03	-1.29E-02	9.04E-03	5.34E-02
Np^{237}	-3.59E-03	-1.41E-02	8.04E-03	5.34E-02

Table 7. Capture rates variations by GPT for different radial positions in TAPIRO.

The results show that, depending on the measurement position in TAPIRO, the effects on the MAs capture rates are different, and for the considered Cu cross sections perturbation, less than 6% in absolute value.
The sensitivity coefficients are shown in Figures 15 through 18.

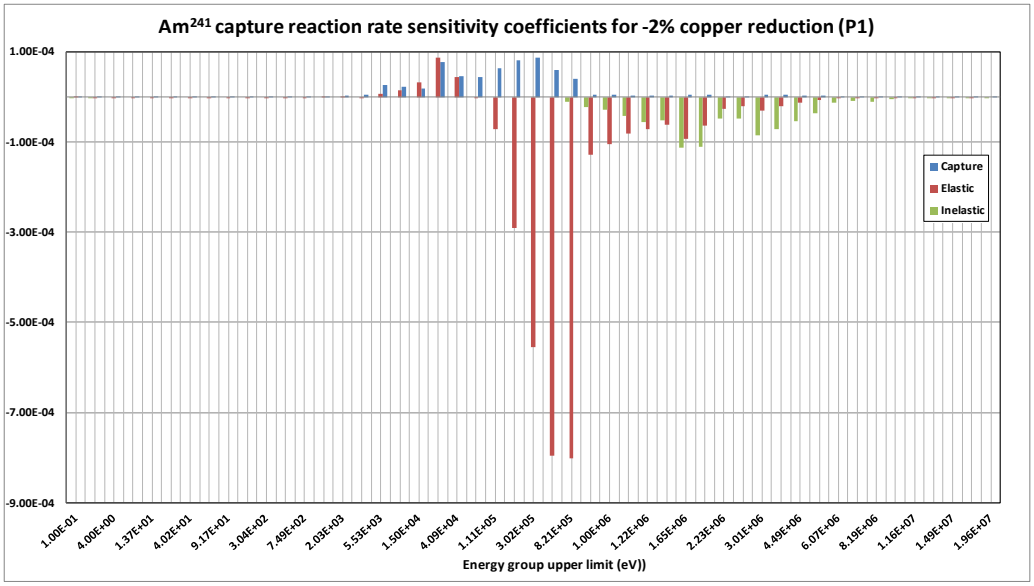

a)

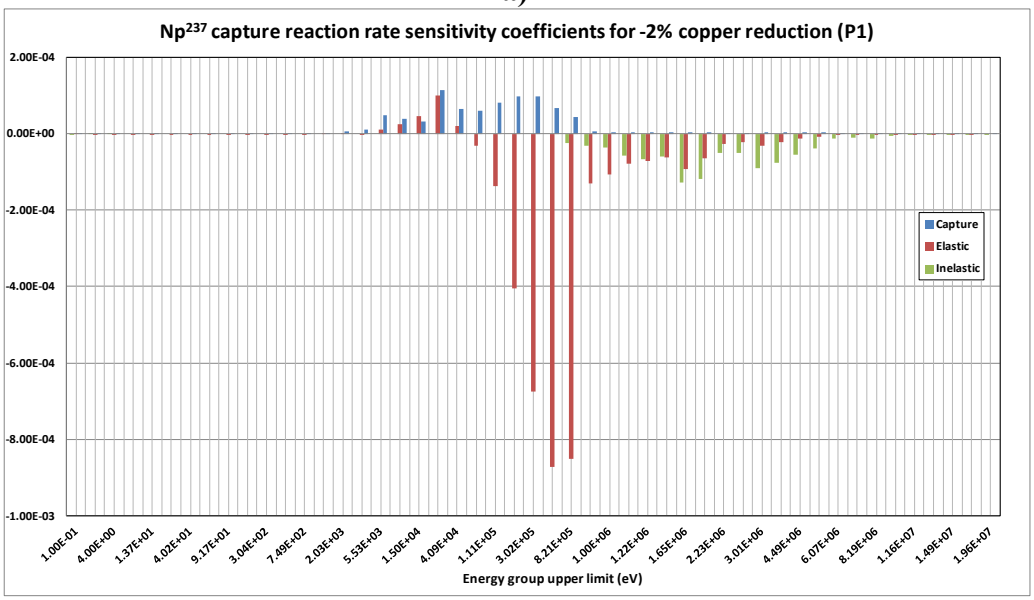

b)

Figure 15: Am^{241}(a) and Np^{237}(b) capture reaction rate sensitivity coefficients in position P1.

The sensitivity coefficients in the central core position for both nuclides, Figure 6, show that the main contribution to the capture rate reduction is due to the copper elastic scattering reactions, the influence of capture and inelastic scattering being negligible.

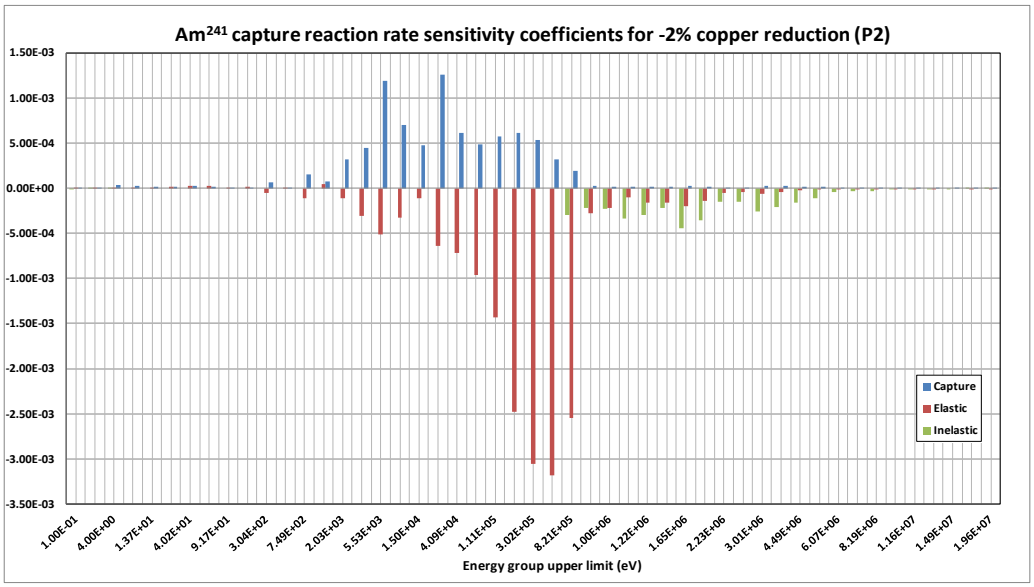

a)

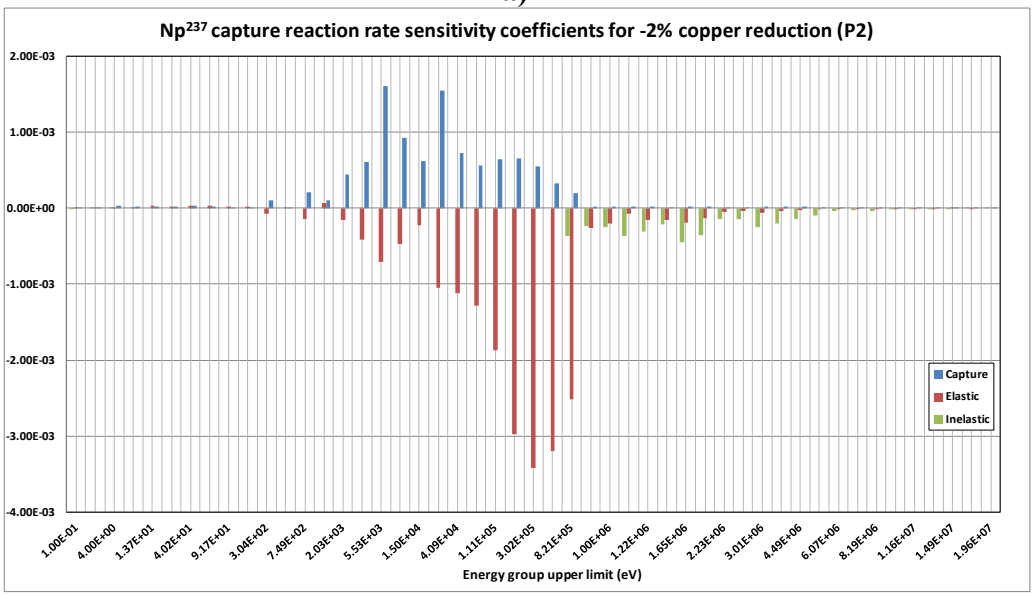

b)

Figure 16: Am^{241}(a) and Np^{237} (b) capture reaction rate sensitivity coefficients in position P2.

The positive influence of the capture reactions start to be evident in the copper reflector at 12.07 cm from the core center, as shown in Figure 7 for both nuclides, even if the main contribution to the variation is due to the elastic scattering reactions.

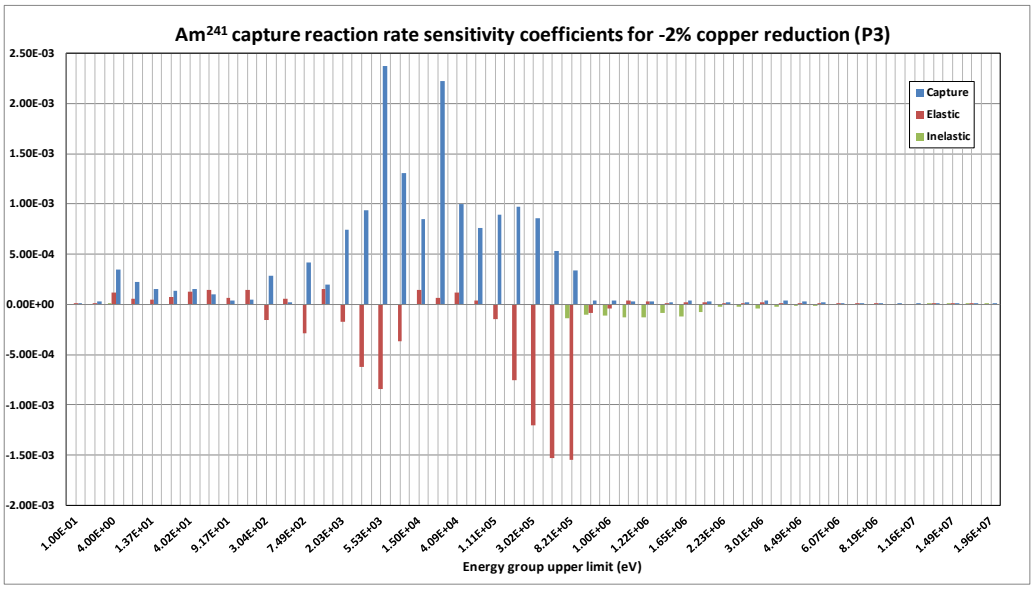

a)

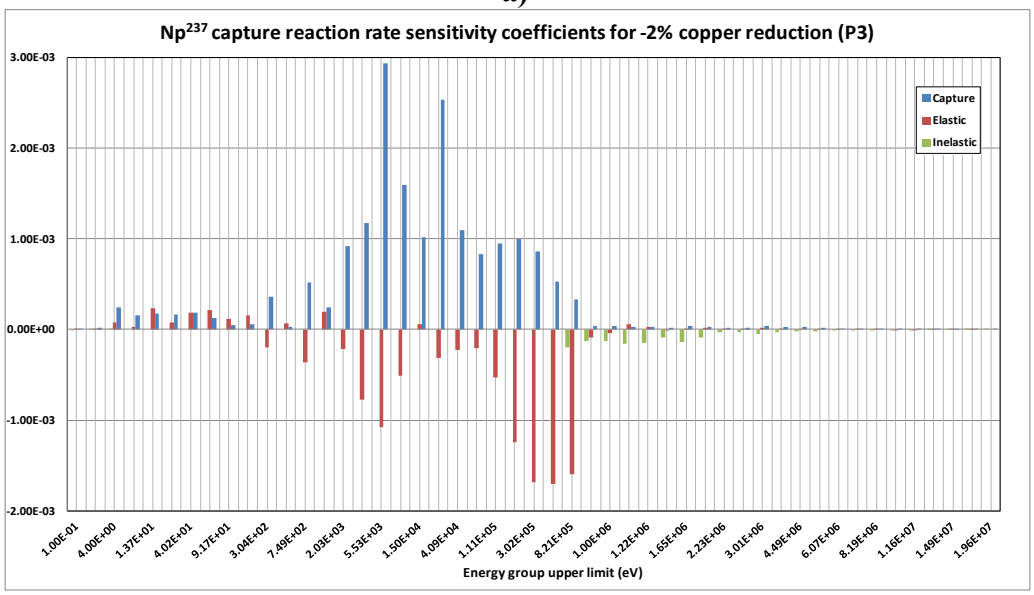

b)

Figure 17: Am^{241}(a) and Np^{237} (b) capture reaction rate sensitivity coefficients in position P3.

In the reflector central position there is a change in the total variation that now is positive (cf. Table 3), and mainly due to the capture reactions even if the elastic scattering contribution is not negligible and in the opposite direction (i.e. negative).

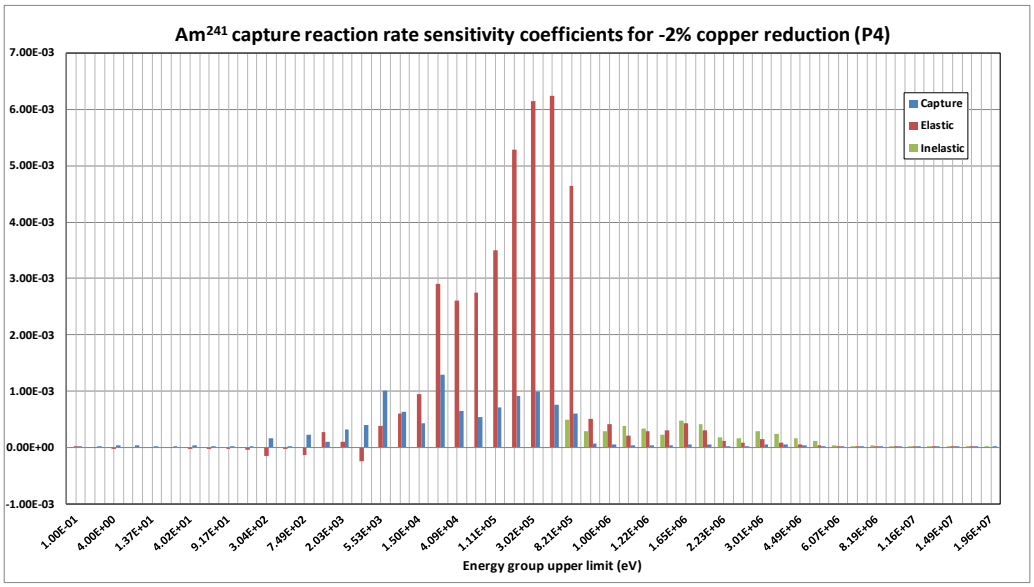

a)

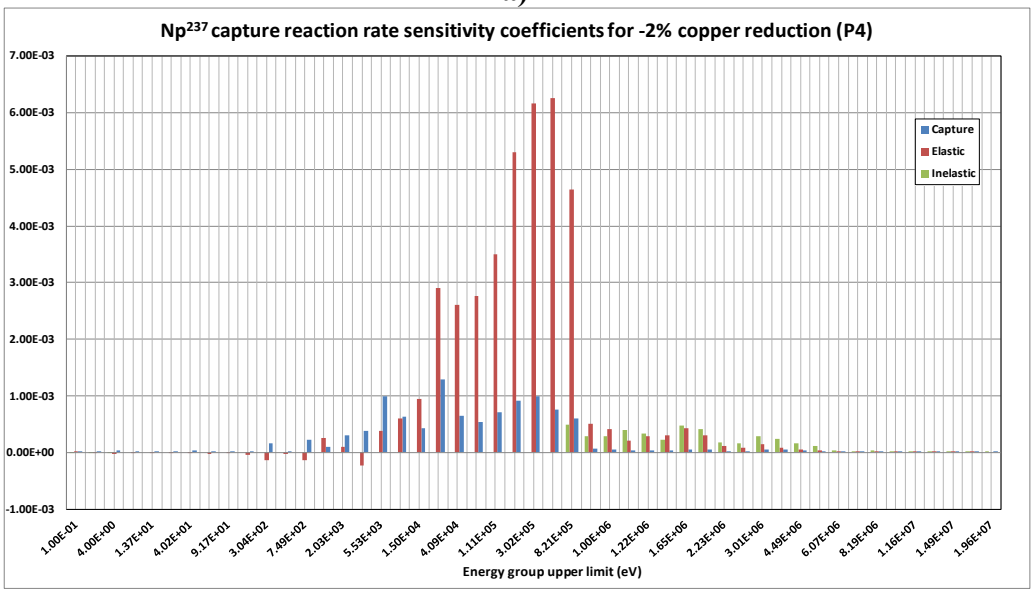

b)

Figure 18: Am^{241} (a) and Np^{237} (b) capture reaction rate sensitivity coefficients in position P4.

At the entrance of the thermal column there is a positive contribution for all the reactions, the main contribution to the total sensitivity being due to elastic scattering reactions.
In all the cases considered the variation is mainly influenced by elastic scattering and capture reactions in the energy range from 20 eV to 800 keV.
By means of a direct approach (direct calculations of unperturbed and perturbed systems) the capture reaction rates for both Am^{241} and Np^{237} have been evaluated for all the different positions along the diametral channel and have been compared with the total sensitivities evaluated by means of GPT, Tables 8 and 9.

	Am^{241}			
Position	0.5 cm	12.07 cm	24.58 cm	45.5 cm

Isotope				
GPT	-3.24E-03	-1.29E-02	9.04E-03	5.34E-02
Direct	-3.14E-03	-1.33E-02	8.76E-03	5.58E-02

Table 8. GPT and direct approach results comparison for Am^{241}.

	Np237			
Position / Isotope	0.5 cm	12.07 cm	24.58 cm	45.5 cm
GPT	-3.59E-03	-1.41E-02	8.04E-03	5.34E-02
Direct	-3.51E-03	-1.48E-02	7.48E-03	5.59E-02

Table 9. GPT and direct approach results comparison for Np^{237}.

The results show a very good reconstruction of the integral effects by the GPT methodology.

8. Experimental campaigns.

The AOSTA (Activation of OSMOSE Samples in TApiro) campaign, in collaboration with CEA, is made of a preliminary neutronic characterization phase of the TAPIRO irradiation channels (Phase 1) useful for the MA cross-section evaluation. The neutron spectrum and flux in several positions are measured making use of the multiple foils activation technique.
Additional measurements will be carried out in this phase by fission chambers (candidates ^{235}U, ^{238}U, ^{237}Np) furnished by CEA and by ENEA measurement chains. For these measurements the reference monitor position will be also chosen.
A second phase (Phase 2), consisting of the AOSTA campaign with MA samples in support of nuclear data improvement, will be performed on the basis of the measurements results obtained in the Phase 1.

Due to the COVID situation, all activities at TAPIRO, and so even the AOSTA campaign has been a delay of 2 years and the restoring of the TAPIRO activities in the framework of the ENEA-CEA AOSTA agreement further delayed the planning. So, only in Fall 2021 the characterization campaign started.
Another stop occurred to the ENEA facilities due to the lack of the nuclear liability insurance. So, any activity could not be performed until September 2023 when the administrative problem has been solved (re-scheduling of the TAPIRO backload). Only recently (in 2024), the activity resumed with priorities given to the backload accumulated.
Currently the AOSTA Phase 1 (TAPIRO experimental channel characterization) is planned to be concluded as soon as the reactor planning allows it.
About Phase 2 of the AOSTA campaign, some MA samples have been already delivered to ENEA Casaccia, and discussions are going on with CEA to define the planning for the delivery of the other MA samples and their irradiations in the framework of the AOSTA Programme.

The phase 1 experimental campaign includes online measurements by means of various fission chambers and activation analysis by means of selected metallic foils.

The selected experimental channels, radial channel 1 and 2 and tangential channel, are equipped with plugs that can be used for online measurements just removing a coaxial rod, ensuring the necessary shielding.

October 2021 fission chamber measurements

The experimental campaign dedicated to measurements with miniature fission chambers (MFC) was realized from 18 to 22 October 2021 with the participation of CEA and ENEA staff.
Measurements were performed with the four MFC listed in Tab.10 located in the TAPIRO tangential channel (TC).
In October 2021, because of operation constraints linked to radioprotection, only two irradiation channels could be used:

- the tangential channel was partially available, between the central area of the reactor and the exit located closed to the channel 2;
- the radial channel 2 was fully available.

In May and June 2022, in the same way, only the tangential channel and the radial channel 2 were used.
Even if this configuration limits the number of available irradiation sites, it allows the access to very interesting irradiation sites for the AOSTA experiment in the tangential channel, where samples can be placed close to the core center, in a high neutron flux and a rapid spectrum, as shown in reference [19].
Furthermore, the radial channel 2 allows the irradiation of a detector used as a monitor or a reference, simultaneously with samples placed in the tangential channel.
In October 2021, the reactor power was limited to 1 kW for a few hours, and then to 10 W, because of operation constraints on the cooling system.
On one hand, the limitation to 1 kW instead of 5 kW allowed characterization irradiations for AOSTA phase 1, even if the irradiations times should be slightly adapted to reach the targeted measurement accuracy.
On the other hand, the limitation to 10 W implied to increase significantly the irradiation time to get satisfying characterization measurements and to adapt the experiment planning.
For the phase 1 of AOSTA, the use of fission chambers was planned to measure fission rates and spectrum indexes. Ten fission chambers, provided by the CEA, were sent to TAPIRO in 2020 and 2021. Five of them were used in October 2021 for characterization measurements (see following Table 10).

Reference	Isotope	Type	Nominal Mass (µg)	Calibrated	Used in October 2021
n°2250	Uranium 235	CF4	5	Yes	Yes
n°2135	Uranium 238	CF4	348	Yes	Yes
n°2236	Neptunium 237	CF4	928,0	Yes	Yes
n°2239	Neptunium 237	CF4	558,0	No	No
n°2240	Neptunium 237	CF4	693	No	No
n°2238	Plutonium 239	CF4	25.5	Yes	Yes (Monitor)
n°2300	Americium 241	CF4	150	No	No
n°2284	Uranium 235	CF8gr	3000	Yes	No
n°2281	Uranium 238	CF8gr	3000	Yes	Yes
n°2283	Neptunium 237	CF8gr	912	Yes	No

Table 10: Fission chambers provided by CEA, available for TAPIRO characterization.

More details about these fission chambers and the associated acquisition system are available in reference [20].

For each MFC measurement in the tangential channel, a MFC, used as monitor and placed in the radial channel 2 (RC2), was simultaneously measured. The MFC used as monitor was MFC 2238, made of 25.5 µg of plutonium 239.
Different types of measurements were performed:

- measurements with a MFC in different positions in the tangential channel, with a monitor staying at the same position in the radial channel 2, to study the fission rates in several TC irradiation positions;
- measurements with the monitor in different positions in the radial channel 2, the other MFC staying at the same position in the tangential channel, to determine the best RC2 position for the monitor (i.e. with a satisfying signal quality) and to be able to estimate the measurement uncertainty associated to the monitor position;
- repeatability measurements in the tangential channel, a MFC being measured in the same TC position several times, and the monitor staying at the same RC2 position.

These measurements were performed by a CEA team of three physicists, in collaboration with the ENEA TAPIRO operating team. This campaign was also an opportunity to share the information about the MFC measurement so that the ENEA team can performed later additional MFC experiments on TAPIRO.
The planned schedule had to be adapted because of operating constraints:

- at the beginning of the campaign, the reactor stopped several times because of parasitic signals in the electronic modules of control command system and it was not possible to run enough time at a steady state power to register satisfying measurements with the fission chambers;
- later, a dysfunction of the secondary loop of the reactor was detected after the 1 kW run, which constrained the ENEA team to run the reactor at a lower power for the rest of the week.

Consequently, some measurements, which were initially scheduled, could not be performed: this is the case of the measurements with plutonium 239 in the tangential channel.

May and June 2022 activation foils measurements.

The core characterization prior to irradiation experiments includes the analysis by means of the activation foils technique. The irradiation of metal foils was realized on TAPIRO, by ENEA team, in May and June 2022, to perform preliminary activation measurements and characterize the neutron flux of the reactor. The neutron activation technique is used to measure the intensity, the energy spectrum, and the spatial distribution of the neutron flux. The reactions have been chosen so to cover the whole energy range of the flux spectrum allowing for unfolding techniques of the neutron spectrum.
This standard technique makes profit of the activation of selected samples in a neutron field, such activation being proportional both to the neutron flux and the detector nuclear characteristics (cross-sections).

For what concerns the measure of the neutron flux level and energy spectrum, unfolding methods are usually employed. In order to apply this approach many reaction rates types (continuous, threshold), sensitive to different energy ranges have to be employed. The ideal goal, of course, is to cover as much as possible the full domain of the energy spectrum characteristic of the facility under examination.

The energy multigroup neutron flux is obtained by the unfolding procedure on the basis of the effective multigroup cross sections values derived by a MC guess spectrum.
To assess and validate predictions of the TAPIRO Monte Carlo modelling, a preliminary characterization campaign is foreseen. Its objectives focus on assessing the neutron spectra in the radial, tangential and diametral channels.
Several measurement techniques should be used and cross-compared:

- Spectral indices with calibrated miniature fission chambers (typically ^{238}U fission rate over ^{235}U fission rate). Detectors from CEA, JAEA and INL could be used to produce complementary results.
- Axial flux distribution measured with miniature fission chambers (^{235}U, ^{238}U, ^{237}Np).
- Reactor dosimetry using metallic activation foils measured by gamma spectroscopy.

With the 'initial guess' for the neutron spectrum by MCNP, activation foils to be used in the experimental trial have been selected (see Tab.11).
The driving criterion utilized for the planning of the experiment trial #1 is "activate foils at the minimum measurable values in gamma spectrometry". The main reason about this choice was due to radiation protection issues.

Reaction utilized	Element target	Outcome radionuclide $T_{1/2}$	irradiation time proposed, 1 kW, y=0	Target type	foil mass [mg]	foil diameter [mm]	A_{real} end irradiation [Bq] 1 kW
Al27naNa24	Al	15 h	60 min	AuAl 11.31%	3	3	2.90E+01
Al27npMg27		10 min					3.37E+03
Au197ngAu198	Au	3 g	60 min				9.44E+02
Co59n2nCo58	Co	71 g	120 min	Co	18.3	5	4.56E+01
Co59naMn56		3 h					1.86E+02
Co59ngCo60		5:00 AM					3.40E+01
Cu63n2nCu62	Cu	10 min	60 min	Cu	5.7	3	4.60E+01
Cu63naCo60		5:00 AM					3.80E-03
Cu63naCo60m		11 min					1.74E+02
Cu63ngCu64		13 h					1.09E+04
Fe54naCr51	Fe	28 g	120 min	Fe	3.8	5	6.40E-02
Fe54npMn54		312 g					5.92E-01
Fe56npMn56		3 h					2.24E+02
Fe58ngFe59		45 g					1.56E-01
In115ngIn116m	In	1 h	60 min	In	3.6	3	5.52E+05
In115nnIn115m		4 h					1.44E+04
Ni58n2nNi57	Ni	1 g	120 min	Ni	86	5	1.04E+00
Ni58npCo58		71 g					6.73E+02
Ni58npnCo57		272 g					4.76E-01
Ni60npCo60		5:00 AM					2.08E-01
Ti46npSc46	Ti	84 g	120 min	Ti	9	5	1.12E+00
Ti47npSc47		3 g					5.02E+01
Ti48npSc48		2 g					1.20E+01
Zn64npCu64	Zn	13 h	60 min	Zn	3.5	5	5.52E+02

Tab. 11 - Targets selection and following reactions used in trial #1.

The evaluation of the A_{real} activities at the end of the irradiation were obtained by means of the FISPACT activation code [7], using the initial spectrum calculated by MCNP as input data to foils activation.

Diameters and masses of foils have been optimized to obtain a 'sufficient' final activation A_{real}, at about ~1 kBq. As to keep 'short lived' radionuclides at these final values, it has been chosen to divide the irradiation foils in two batches:

- Short irradiation, 60 minutes:
  - Zn, 5mm,
  - Au-Al 11.31%, 3 mm,
  - Cu, 3 mm,
  - In, 3 mm;
- Long irradiation, 120 minutes:
  - Co, 5mm,
  - Fe, 5 mm,
  - Ni, 5 mm,
  - Ti, 5 mm.

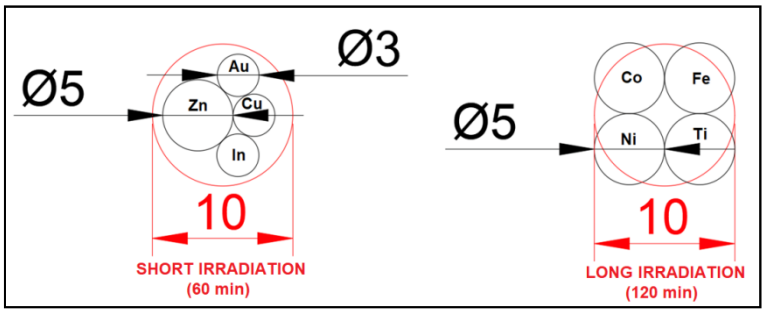

Fig. 19 – Irradiation batches, short (60 minutes) and long (120 minutes).

Each batch of foils have been wrapped to external surface of two different stainless-steel tubes, and got irradiated with the following schedule:

- Short irradiation, July 13th, beginning 10:57, end 11:58, total duration 61 minutes;
- Long irradiation, July 13th, beginning 12:01, end 14:01, total duration 120 minutes.

The activation of foils being designed to be as small as possible (about ~1 kBq per radionuclide), the most critical issue identified about the activated samples management is regarding the decay of short-lived radionuclides. Because of this physical decay, and the need to characterize the samples in gamma spectrometry before decaying, no cooling is foreseen for the 'short-lived' batch. The sample management has been done just after the extraction from reactor TC, with a contact H*(10) dose rate of about ~2-3 mSv/h.
Long irradiation batch does not have such decaying issue, and a cooling time allowed to reduce H*(10) dose rate at contact.
At the moment of the experiment, only one Canberra GX5020 HPGe detector was available, and foil measurements have been carried sequentially, following the activity evolution vs. time of different radionuclides to be determined.
Total calibration of the detector has been achieved with certified standard Eu-152 sources:

- NIST SRM 4218F-19 Eu-152 point source, 99.21 ± 0.4 kBq (28/07/2022 12:00 UT -2h Rome Time, uncertainty 1s);
- INMRI Institute SP-2070 Eu-152 point source, 2087.49 ± 16.70 Bq (28/07/2022 12:00 UT -2h Rome Time, uncertainty 1s).

The final characterization results of activation foils have been resumed, Tab.

					Calculated values		Measured values	
Reaction utilized	Element target	Outcome radionuclide $T_{1/2}$	irradiation time proposed, 1 kW, y=0	Target type	A_{real} end irradiation 1 kW [Bq]	A_{real} end irradiation 1 kW [Bq/atom]	A_{real} end irradiation 1 kW [Bq/atom]	Uncertainty 1s [%]
Al27naNa24	Al	15 h	60 min	AuAl 11.31%	2.90E+01	1.08E-17	1.06E-17	13%
Al27npMg27		10 min			3.37E+03	5.75E-17	7.28E-17	3%
Au197ngAu198	Au	3 g	60 min		9.44E+02	8.54E-14	1.86E-13	10%
Co59n2nCo58	Co	71 g	120 min	Co	4.56E+01	3.00E-16	< MDA	
Co59naMn56		3 h			1.86E+02	2.39E-18	3.07E-18	7%
Co59ngCo60		5:00 AM			3.40E+01	6.07E-15	1.59E-14	6%
Cu63n2nCu62	Cu	10 min	60 min	Cu	4.60E+01	1.25E-18	< MDA	
Cu63naCo60		5:00 AM			3.80E-03	6.78E-18	< MDA	
Cu63naCo60m		11 min			1.74E+02	1.06E-17	< MDA	
Cu63ngCu64		13 h			1.09E+04	5.51E-15	5.41E-15	17%
Fe54naCr51	Fe	28 g	120 min	Fe	6.40E-02	1.28E-17	< MDA	
Fe54npMn54		312 g			5.92E-01	1.34E-15	< MDA	
Fe56npMn56		3 h			2.24E+02	1.43E-17	2.25E-17	10%
Fe58ngFe59		45 g			1.56E-01	1.04E-15	< MDA	
In115ngIn116m	In	1 h	60 min	In	5.52E+05	5.71E-14	6.92E-14	9%
In115nnIn115m		4 h			1.44E+04	5.56E-15	6.48E-15	4%
Ni58n2nNi57	Ni	1 g	120 min	Ni	1.04E+00	4.56E-20	< MDA	
Ni58npCo58		71 g			6.73E+02	1.37E-15	2.31E-15	7%
Ni58npnCo57		272 g			4.76E-01	3.73E-18	< MDA	
Ni60npCo60		5:00 AM			2.08E-01	3.00E-17	< MDA	
Ti46npSc46	Ti	84 g	120 min	Ti	1.12E+00	1.74E-16	3.28E-16	35%
Ti47npSc47		3 g			5.02E+01	3.48E-16	4.46E-16	13%
Ti48npSc48		2 g			1.20E+01	4.60E-18	5.13E-18	14%
Zn64npCu64	Zn	13 h	60 min	Zn	5.52E+02	2.55E-16	9.27E-16	21%

Table 12.

					Calculated values		Measured values	
Reaction utilized	Element target	Outcome radionuclide $T_{1/2}$	irradiation time proposed, 1 kW, y=0	Target type	A_{real} end irradiation 1 kW [Bq]	A_{real} end irradiation 1 kW [Bq/atom]	A_{real} end irradiation 1 kW [Bq/atom]	Uncertainty 1s [%]
Al27naNa24	Al	15 h	60 min	AuAl 11.31%	2.90E+01	1.08E-17	1.06E-17	13%
Al27npMg27		10 min			3.37E+03	5.75E-17	7.28E-17	3%
Au197ngAu198	Au	3 g	60 min		9.44E+02	8.54E-14	1.86E-13	10%
Co59n2nCo58	Co	71 g	120 min	Co	4.56E+01	3.00E-16	< MDA	
Co59naMn56		3 h			1.86E+02	2.39E-18	3.07E-18	7%
Co59ngCo60		5:00 AM			3.40E+01	6.07E-15	1.59E-14	6%
Cu63n2nCu62	Cu	10 min	60 min	Cu	4.60E+01	1.25E-18	< MDA	
Cu63naCo60		5:00 AM			3.80E-03	6.78E-18	< MDA	
Cu63naCo60m		11 min			1.74E+02	1.06E-17	< MDA	
Cu63ngCu64		13 h			1.09E+04	5.51E-15	5.41E-15	17%
Fe54naCr51	Fe	28 g	120 min	Fe	6.40E-02	1.28E-17	< MDA	
Fe54npMn54		312 g			5.92E-01	1.34E-15	< MDA	
Fe56npMn56		3 h			2.24E+02	1.43E-17	2.25E-17	10%
Fe58ngFe59		45 g			1.56E-01	1.04E-15	< MDA	
In115ngIn116m	In	1 h	60 min	In	5.52E+05	5.71E-14	6.92E-14	9%
In115nnIn115m		4 h			1.44E+04	5.56E-15	6.48E-15	4%
Ni58n2nNi57	Ni	1 g	120 min	Ni	1.04E+00	4.56E-20	< MDA	
Ni58npCo58		71 g			6.73E+02	1.37E-15	2.31E-15	7%
Ni58npnCo57		272 g			4.76E-01	3.73E-18	< MDA	
Ni60npCo60		5:00 AM			2.08E-01	3.00E-17	< MDA	
Ti46npSc46	Ti	84 g	120 min	Ti	1.12E+00	1.74E-16	3.28E-16	35%
Ti47npSc47		3 g			5.02E+01	3.48E-16	4.46E-16	13%
Ti48npSc48		2 g			1.20E+01	4.60E-18	5.13E-18	14%
Zn64npCu64	Zn	13 h	60 min	Zn	5.52E+02	2.55E-16	9.27E-16	21%

Table 12 - Final results of activation foil reactions characterization used in trial #1.

The total characterization of activated foils has been realized by acquisition of 84 spectra in about 10 days after irradiation, so that the complete reactor dosimetry exercise could fit in two weeks from the irradiation day on.

With the activation foils utilized, and characterization efforts carried out, 14 reactions have been acknowledged to initiate the spectral adjustment process to determine the best estimate of the neutron energy spectrum.
Figure 20 shows the comparison of the spectra obtained with STAYSL [16], SAND-II [17], and NLLSUP [18] with the initial trial spectrum from MCNP. Uncertainties (1s) for STAYSL and NLLSUP codes have been reported as error bars in the graphical comparison. Being the Monte Carlo neutron spectrum calculated with the TAPIRO "0" model which is different from the real implemented geometry, MCNP uncertainties in the spectral comparison are not reported. The SAND-II code, with the version available for the reactor staff, does not report uncertainties in calculation. Within their uncertainties, STAYSL and NLLSUP results show to be compatible each other.
The peak shape of the STAYSL spectrum reproduces the trial spectrum feature of having a maximum followed by a shoulder at slightly higher energy. However, it overestimated the intensity of the whole peak structure. Conversely, the NLLSUP result is closer to the trial

intensities in the peak zone but relocated the maximum at the energy of the trial's shoulder. Finally, SAND-II shows a spectrum that reduces the spectra intensity relative to the trial.
The differences between the STAYSL and SAND-II and the SAND-II algorithm-based NLLSUP code can be ascribed to the different type of algorithm and cross section used. Instead, the difference between SAND-II and NLLSUP can be attributed to the different cross sections and their treatment. In fact, SAND-II uses cross sections integrated on a 620 energy groups whereas NLLSUP use the last version of IRDF-II pointwise cross sections. STAYSL uses the same IRDF-II data with respect to NLLSUP, but with a different adjustment algorithm.

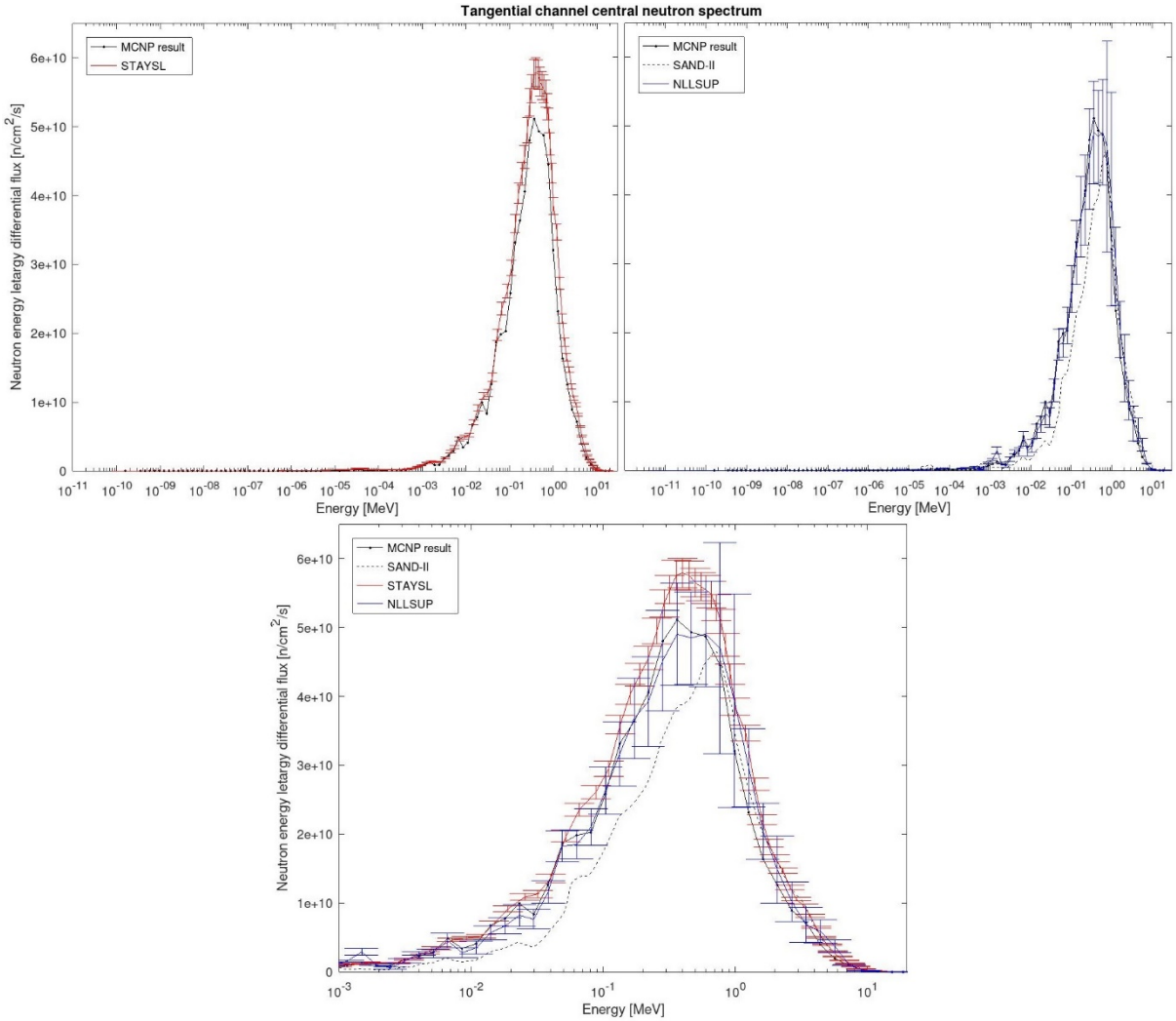

Fig. 20 - Neutron spectra obtained in the unfolding procedure using STAYSL, SAND-II, and NLLSUP codes and their comparison with the input trial spectrum from the MCNP simulation of the TAPIRO reactor in the central position of the tangential channel.

Figure 20 - Neutron spectra obtained in the unfolding procedure using STAYSL, SAND-II, and NLLSUP codes and their comparison with the input trial spectrum from the MCNP simulation of the TAPIRO reactor in the central position of the tangential channel.

Results obtained from the ENEA R.S.V. TAPIRO reactor dosimetry, Tangential Channel, y=0, 1 kW thermal power, trial #1 have been considered a successful experience by the reactor staff due to:

- demonstration of the feasibility of the 'fast calibration procedure' i.e. the capability to obtain an experimentally determined fast neutron spectrum in a relatively short time, about two weeks;
- radiation protection goals, i.e. keep the operator exposure while managing activated sample holder and foils during the characterization campaign in a total Effective Dose value less than 100 μSv per experiment;
- keep the activation foils set in a limited number of items and irradiation batches, as to simplify the irradiation procedure and all following actions, producing an even valuable spectral result.

Aspects acknowledged to be enhanced in future experience are related to the radiological characterization of activated foils, in order to reduce uncertainties and to increase the accuracy of saturation activities determined.

9. Preliminary analysis of the measurements

Fission chamber measurement

The first analyses of the experiments performed with fission chambers in 2021 show a good consistency of the measurements, especially about the evolution of the counting rate as a function of the distance between the detector and the core center. They show also a satisfying repeatability.
The following figures 21 and 22, from [20], are given as an illustration.

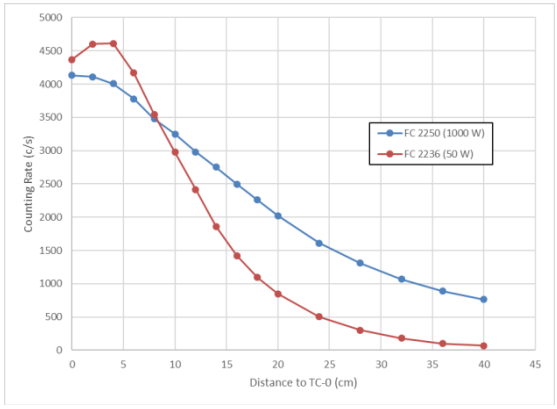

Figure 21: Counting rates of fission chambers 2250 (uranium 235) at 1000 W and 2236 (neptunium 237) at 50 W in the tangential channel of TAPIRO, as a function of the distance toTC-0.

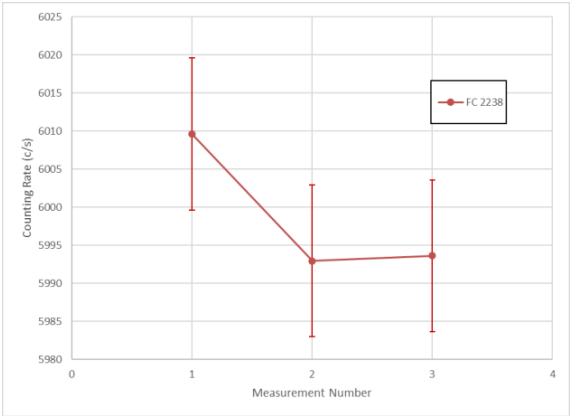

Figure 22: Counting rates of the fission chamber 2238 (plutonium 239), at 1000 W, in the radial channel 2 (repeatability measurements).

The measured counting rates of fission chamber N°2250 (uranium 235) and n°2236 (neptunium 237), presented in the previous section were normalized to the value at point of the tangential channel, which is the closest to the reactor center. Then, these normalized experimental counting rates were compared to calculated reaction rates, normalized at the same point. Results are displayed in the following Table 13, Figure 23 and Figure 24.

Distance to the Closest Point to the Reactor Center (cm)	Fission Chamber 2250 (Uranium 235)			Fission Chamber 2236 (Neptunium 237)		
	Measurement (E)	Calculation (C)	C/E-1	Measurement (E)	Calculation (C)	C/E-1
0	1	1	0%	1	1	0%
2	0.994			1.053		
4	0.97	0.831	-14%	1.055	0.792	-25%
6	0.914			0.953		
8	0.841	0.487	-42%	0.812	0.311	-62%
10	0.787			0.681		
12	0.722	0.315	-56%	0.552	0.12	-78%
14	0.667			0.426		
16	0.605	0.235	-61%	0.326	0.059	-82%
18	0.546			0.251		
20	0.489	0.177	-64%	0.194	0.031	-84%
24	0.39	0.133	-66%	0.115	0.017	-86%
28	0.317	0.102	-68%	0.069	0.009	-87%
32	0.259	0.082	-68%	0.041	0.005	-88%
36	0.215	0.068	-68%	0.023	0.003	-88%
40	0.184	0.063	-66%	0.016	0.003	-91%
44		0.064			0.001	

Table 13: Normalized reaction rates of fission chambers 2250 (uranium 235) and 2236 (neptunium 237), in the tangential channel of TAPIRO, as a function of the distance to the closest point to the reactor center.

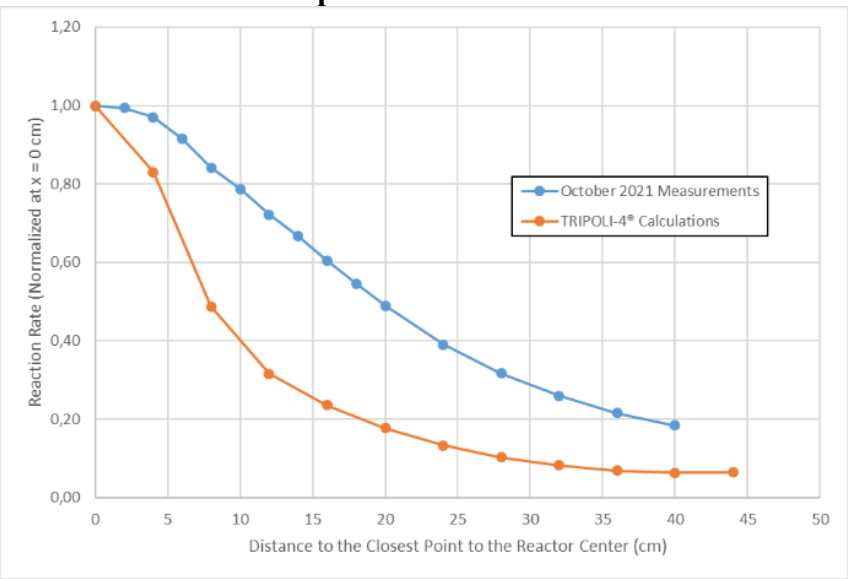

Figure 23: Reaction rates of fission chamber 2250 (uranium 235) in the tangential channel of TAPIRO, as a function of the distance to the closest point to the reactor center.

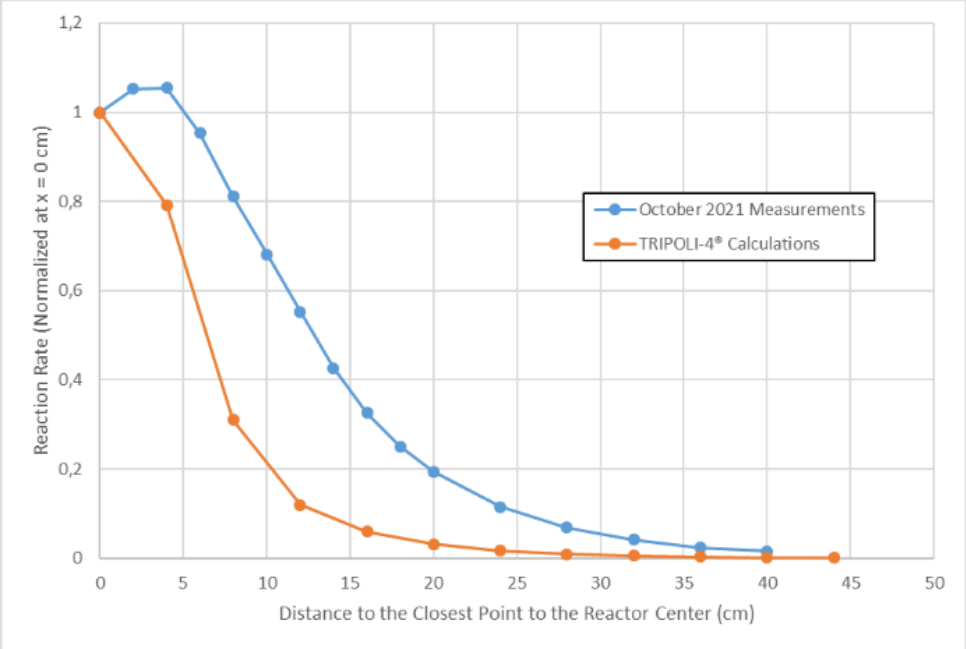

Figure 24: Reaction rates of fission chamber 2236 (neptunium 237) in the tangential channel of TAPIRO, as a function of the distance to the closest point to the reactor center.

The calculated reaction rates decrease when the distance to the core center increases: this is globally consistent with the evolution of the experimental reaction rates. However, the light increase at small distances observed for measurements on the neptunium 237 fission chamber does not appear in the calculations. Moreover, the calculated reaction rates significantly underestimate the experimental values: the difference is moderate at short distances: from 14 % to 25 % up to 4 cm, but it is higher at long distances.
These differences have to be investigated. It would be interesting to get activation measurements in the tangential channel, at several distances to the core center, and to evaluate the evolution of the experimental and calculated reaction rates as a function of the distance to the core center, to test the model used in the simulation.

Comparison of activation measurements with simulation results

The experimental saturated activities were compared with MCNP simulation results provided by the ENEA. These simulations were performed using the JEFF 3.3 nuclear data library. They are displayed in the following Table 10.

Activation Reaction	Saturation Activity (Bq/at)		C/E-1
	Measurement (E)	MCNP Simulation (C)	
$^{27}Al(n,alpha)^{24}Na$	1.38×10^{-17}	1.08×10^{-17}	-22%
$^{27}Al(n,p)^{27}Mg$	9.73×10^{-17}	5.75×10^{-17}	-41%
$^{197}Au(n,gamma)^{198}Au$	2.25×10^{-13}	8.54×10^{-14}	-62%
$^{63}Cu(n,gamma)^{64}Cu$	7.03×10^{-15}	5.51×10^{-15}	-22%
$^{115}In(n,gamma)^{116}mIn$	7.33×10^{-14}	5.71×10^{-14}	-22%
$^{115}In(n,n)^{115}mIn$	9.21×10^{-15}	5.56×10^{-15}	-40%
$^{115}In(n,2n)^{114}mIn$	5.96×10^{-15}	2.29×10^{-15}	-62%
$^{64}Zn(n,p)^{64}Cu$	1.18×10^{-15}	2.55×10^{-16}	-78%
$^{59}Co(n,alpha)^{56}Mn$	3.31×10^{-18}	2.39×10^{-18}	-28%
$^{59}Co(n,gamma)^{60}Co$	1.98×10^{-14}	6.07×10^{-15}	-69%
$^{56}Fe(n,p)^{56}Mn$	2.51×10^{-17}	1.47×10^{-17}	-41%
$^{58}Ni(n,p)^{58}Co$	2.83×10^{-15}	1.37×10^{-15}	-52%
$^{46}Ti(n,p)^{46}Sc$	3.47×10^{-16}	1.74×10^{-16}	-50%
$^{47}Ti(n,p)^{47}Sc$	6.44×10^{-16}	3.48×10^{-16}	-46%
$^{48}Ti(n,p)^{48}Sc$	6.23×10^{-18}	4.60×10^{-18}	-26%

Table 14: Comparison of the measured saturation activities with ENEA MCNP simulation results.

The orders of magnitude of the experimental and simulated saturated activities displayed in the Table 14 are the same. The differences of several ten of percent are consistent with the experimental uncertainties.

However, there seems to be a bias between the measurements and the calculations as the MCNP results systematically underestimate the experimental results. This could be explained by an imperfect evaluation of the power of the reactor. This evaluation, made using the control room devices, could be improved using additional monitors in potential future experiments: reference fission chambers or reference activation foils.

The activation measurements and MCNP calculations displayed in Table 14 were normalized to the gold foil activation, so that they can be compared to TRIPOLI-4® activities evaluated from reaction rates given in reference [19]. The experimental and computed normalized saturation activities are displayed in the following Table 11.

Activation Reaction	Saturation Activity (Bq/at), normalized to gold			C/E-1	
	Measurement (E)	MCNP (C)	TRIPOLI-4® (C)	MCNP	TRIPOLI-4®
$^{27}Al(n,alpha)^{24}Na$	6,13E-05	1,26E-04	1,30E-04	106%	113%
$^{27}Al(n,p)^{27}Mg$	4,32E-04	6,73E-04		56%	
$^{197}Au(n,gamma)^{198}Au$	1,00E+00	1,00E+00	1,00E+00	0%	0%
$^{63}Cu(n,gamma)^{64}Cu$	3,12E-02	6,45E-02		107%	
$^{115}In(n,gamma)^{116}mIn$	3,26E-01	6,69E-01		105%	
$^{115}In(n,n)^{115}mIn$	4,09E-02	6,51E-02	2,09E-04	59%	-99%
$^{115}In(n,2n)^{114}mIn$	2,65E-02	2,68E-02		1%	
$^{64}Zn(n,p)^{64}Cu$	5,24E-03	2,99E-03	3,24E-03	-43%	-38%
$^{59}Co(n,alpha)^{56}Mn$	1,47E-05	2,80E-05		90%	
$^{59}Co(n,gamma)^{60}Co$	8,80E-02	7,11E-02	9,77E-02	-19%	11%
$^{56}Fe(n,p)^{56}Mn$	1,12E-04	1,72E-04		54%	
$^{58}Ni(n,p)^{58}Co$	1,26E-02	1,60E-02	2,14E-02	28%	70%
$^{46}Ti(n,p)^{46}Sc$	1,54E-03	2,04E-03	1,92E-03	32%	25%
$^{47}Ti(n,p)^{47}Sc$	2,86E-03	4,07E-03	4,05E-03	42%	41%
$^{48}Ti(n,p)^{48}Sc$	2,77E-05	5,39E-05	4,89E-05	95%	77%

Table 15: Saturation activities normalized to gold, measurements compared to simulations

The TRIPOLI-4® calculation were performed with the version 11 of TRIPOLI-4® and the CEAV512 nuclear data library, based on JEFF-3.1.1 European evaluation. The self-protection effect in the dosimeters was not taken into account in the TRIPOLI-4® calculations. However, the self-protection in the gold foil was evaluated by ENEA, thanks to MCNP calculations, to around 1 %, which proves that this phenomenon has no significant effect on activation evaluation for this experiment.

The MCNP and TRIPOLI-4® results are consistent, with differences lower than 20%, for the activation reactions on aluminum, zinc, and titanium. Differences are higher, up to 42%, for reactions on indium, cobalt and nickel. Taking into account the high experimental uncertainties of several tens of percent, it seems difficult to get a more advanced interpretation of these results.

TRIPOLI-4© results are missing for some activation foils: these calculations were not performed in the preliminary design study presented in reference [19] because they were not identified as potential interesting reactions at this time. Takeing into account the high uncertainties associated to the measurements and the difficulties to analyze the available experimental results, it was considered that was not useful to perform additional calculations to complete the Table 15.

Conclusions

In the frame of the NEA Expert Group on Integral Experiments for Minor Actinide Management, a joint collaboration between ENEA and CEA was established with the aim to study the feasibility of a MAs irradiation campaign, named AOSTA (Activation of Osmose Samples in TApiro), in the TAPIRO fast neutron source research reactor located at the ENEA Casaccia center near Rome.
Results from the deterministic and probabilistic evaluations of the irradiation campaign simulations indicate the feasibility of the AOSTA experimental campaign.
The sensitivity coefficients of the MAs reaction rates to Cu cross section variations have been estimated by means of both Generalized Perturbation Theory (GPT) and direct approach by deterministic calculations. Experimental uncertainties on Cu nuclear data have been simulated, in this preliminary approach, by a uniform change on the Cu reflector density. The results show that, depending on the measurement position in TAPIRO, uncertainties on the Cu nuclear data may play different roles, even as order of magnitude, on the experimental results. Further investigations are needed to find optimal measurement positions with regard to both neutron spectrum entering the samples and influence of Cu cross sections uncertainties on the measured MAs reaction rates.
Due to the COVID situation first, the administrative collaboration definitions and TAPIRO nuclear liability insurance, the Phase 1 AOSTA campaign could not be completed with all the measurements initially proposed. However significant progress has been made to approach validation of the proposed experimental scheme.
The experimental campaign carried out by CEA and ENEA staff in 2021 and 2022 are presented and described, the first preliminary data measured are shown and compared with calculations results, some discrepancies are highlighted. Both CEA and ENEA plan to complete the AOSTA experimental campaign (Phase 1) after the finalization of SANDA, taking advantage of the tests and results obtained within the SANDA EURATOM project. The results produced will be used by the European ND community to further validate relevant cross-sectional data, eventually within the APRENDE project.

REFERENCES

[1] Nuclear Energy Agency website, Expert Group on Integral Experiments for Minor Actinide Management section: https://www.oecd-nea.org/science/ma/.

[2] ENEA, Italian National Agency for New Technology, Energy and Sustainable Economic Development website, TAPIRO Research Reactor section: http://www.enea.it/en/research-development/documents/nuclear-fission/tapiro-eng-pdf

[3] L. Donnet, N. Drin, P. Fougeras, JP. Hudelot, F. Jorion, R. Klann, (2004), "OSMOSE: An Experimental Program for the Qualification of Integral Cross Sections of Actinides", Proc. PHYSOR-2004, Chicago, Illinois.

[4] V. Becares, P. Blase, B. Geslot, A. Gruel, S. Kopecky, P. Leconte, L. Mathieu, G. Noguere, A. Plompen, P. Ros, P. Schillebeeckx, D. Villamarin, (2016), "Americium-241 integral radiative capture cross section in over-moderated neutron spectrum from pile oscillator measurements in the Minerve reactor", Int. Conf. on Nuclear Data (ND 2016), 12-16 June, Brugge, Belgium.

[5] D. Plisson, G. Rimpault, J. Tommasi, J.M. Rieunier, (2002), "The ERANOS code and data system for fast reactor neutronic analyses", Proc. PHYSOR 2002, Seoul, Korea.

[6] M. Carta, P. Blase, C. Bethaz, F. Boccia, V. Fabrizio, B. Gelsot, A. Grossi, A. Gruel (2016), "Feasibility study of the AOSTA experimental campaign", WONDER 2015: Fourth International Workshop on Nuclear Data Evaluation for Reactor Applications, 5-8 October 2015, Aix-en-Provence (France). EPJ Web of Conferences 111, 0700. ISBN: 978-2-7598-1970-6.

[7] R. A. Forrest (2007), "FISPACT-2007: User manual", UKAEA FUS 534, EURATOM/UKAEA Fusion Association, Culham Science Centre.

[8] SERPENT code website: http://montecarlo.vtt.fi

[9] X-5 Monte Carlo Team, (2003 - Revised 10/3/05) "MCNP: A General Monte Carlo Transport Code" LA-CP-03-245.

[10] Denise B. Pelowitz (ed.), (2013), "MCNP6TM User's Manual, Version 1.0", LA-CP-13-00634, Rev. 0.

[11] K.W. Burn (2011), "Optimizing Monte Carlo to Multiple Responses: the Direct Statistical Approach, 10 Years On", Nucl. Technol. 175-1 138-145.

[12] K.W. Burn (2016), P. Console Camprini, "Radiation transport out from the reactor core: to decouple or not to decouple", Proc. of the ICRS-13.

[13] Jeffrey A. Favorite (2009) "On the Accuracy of the Differential Operator Monte Carlo Perturbation Method for Eigenvalue Problems," Trans. of the American Nuclear Society, 101, 460-462, LA-UR-09-4207.

[14] Forrest B. Brown, Brian C. Kiedrowski, Paul P.H. Wilson, (2010), "Adjoint-Weighted Tallies for k-Eigenvalue Calculations with Continuous-Energy Monte Carlo", Nucl. Sci. Eng. 168, 38-50, 2011, LA-UR-10-01824.

[15] A. Gandini, "Generalized Perturbation Theory (GPT) Methods. A Heuristic Approach", in Advances in Nuclear Science and Technology, Vol. 19, Plenum Press, New York, 1987.

[16] USA Pacific NorthWest National Laboratory, "STAYSL PNNL Software Suite for Reactor Dosimetry," [Online]. Available: https://www.pnnl.gov/projects/staysl-pnnl-software-suite-reactor-dosimetry. [Accessed 21 February 2023].

[17] "SAND-II, Neutron Flux Spectra from Multiple Foil Activation Experiment," [Online]. Available: https://www.oecd-nea.org/tools/abstract/detail/ccc-0112/. [Accessed 21 February 2023].

[18] A. Santagata, "NLLSUP Non Linear Least Squares Unfolding Program Version 0.2," July 2007.

[19] Pierre Casoli, Benoit Geslot and Olivier Clamens, "Programme expérimental AOSTA – Phase 1 : note préparatoire à la conception", CEA/DES/IRESNE/DER/SPESI/LP2E/NT/2020/027/indice A, CEA Technical Note, CEA/DES/IRESNE/DER/SPESI/LP2E DO 99, 18/12/2020.

[20] Pierre Casoli, Benoit Geslot and Timothée Kooyman, “Programme expérimental AOSTA – Phase 1 : compte-rendu de la campagne de mesure réalisée du 18 au 22 octobre 2021 pour la caractérisation du réacteur TAPIRO”, SPESI/LP2E/NT/2021/030/indice A, CEA Technical Note, CEA/DES/IRESNE/DER/SPESI/LP2E DO 2021-079, 17/12/2021.